

## RESEARCH ARTICLE

## Examining the efficacy of localised gemcitabine therapy for the treatment of pancreatic cancer using a hybrid agent-based model

Adrienne L. Jenner<sup>1\*</sup>, Wayne Kelly<sup>2</sup>, Michael Dallaston<sup>1</sup>, Robyn Araujo<sup>1</sup>, Isabelle Parfitt<sup>1</sup>, Dominic Steinitz<sup>3,4</sup>, Pantea Pooladvand<sup>5</sup>, Peter S. Kim<sup>5</sup>, Samantha J. Wade<sup>6,7</sup>, Kara L. Vine<sup>6,7</sup>

**1** School of Mathematical Sciences, Queensland University of Technology, Brisbane, Queensland, Australia, **2** School of Computer Science, Queensland University of Technology, Brisbane, Queensland, Australia, **3** Tweag Software Innovation Lab, London, United Kingdom, **4** Kingston University, Kingston, United Kingdom, **5** School of Mathematics and Statistics, University of Sydney, Sydney, New South Wales, Australia, **6** Illawarra Health and Medical Research Institute, Wollongong, New South Wales, Australia, **7** School of Chemistry and Molecular Bioscience, University of Wollongong, Wollongong, New South Wales, Australia

\* [adrienne.jenner@qut.edu.au](mailto:adrienne.jenner@qut.edu.au)



## OPEN ACCESS

**Citation:** Jenner AL, Kelly W, Dallaston M, Araujo R, Parfitt I, Steinitz D, et al. (2023) Examining the efficacy of localised gemcitabine therapy for the treatment of pancreatic cancer using a hybrid agent-based model. *PLoS Comput Biol* 19(1): e1010104. <https://doi.org/10.1371/journal.pcbi.1010104>

**Editor:** Philip K. Maini, Oxford, UNITED KINGDOM

**Received:** April 19, 2022

**Accepted:** December 21, 2022

**Published:** January 17, 2023

**Copyright:** © 2023 Jenner et al. This is an open access article distributed under the terms of the [Creative Commons Attribution License](https://creativecommons.org/licenses/by/4.0/), which permits unrestricted use, distribution, and reproduction in any medium, provided the original author and source are credited.

**Data Availability Statement:** All relevant data are within the manuscript, in the [Supporting Information](#) files, and located on the Github repository <https://github.com/AdrienneJennerQUT/hybrid-VCBM-of-gemcitabine-and-pancreatic-cancer>.

**Funding:** ALJ and IP were funded by the First Byte Funding Scheme from the Centre for Data Science at Queensland University of Technology. ALJ was also funded by a Fonds de recherche du Québec – Santé International Postdoctoral Fellowship, Centre

## Abstract

The prognosis for pancreatic ductal adenocarcinoma (PDAC) patients has not significantly improved in the past 3 decades, highlighting the need for more effective treatment approaches. Poor patient outcomes and lack of response to therapy can be attributed, in part, to a lack of uptake of perfusion of systemically administered chemotherapeutic drugs into the tumour. Wet-spun alginate fibres loaded with the chemotherapeutic agent gemcitabine have been developed as a potential tool for overcoming the barriers in delivery of systemically administered drugs to the PDAC tumour microenvironment by delivering high concentrations of drug to the tumour directly over an extended period. While exciting, the practicality, safety, and effectiveness of these devices in a clinical setting requires further investigation. Furthermore, an in-depth assessment of the drug-release rate from these devices needs to be undertaken to determine whether an optimal release profile exists. Using a hybrid computational model (agent-based model and partial differential equation system), we developed a simulation of pancreatic tumour growth and response to treatment with gemcitabine loaded alginate fibres. The model was calibrated using *in vitro* and *in vivo* data and simulated using a finite volume method discretisation. We then used the model to compare different intratumoural implantation protocols and gemcitabine-release rates. In our model, the primary driver of pancreatic tumour growth was the rate of tumour cell division. We were able to demonstrate that intratumoural placement of gemcitabine loaded fibres was more effective than peritumoural placement. Additionally, we quantified the efficacy of different release profiles from the implanted fibres that have not yet been tested experimentally. Altogether, the model developed here is a tool that can be used to investigate other drug delivery devices to improve the arsenal of treatments available for PDAC and other difficult-to-treat cancers in the future.

for Applied Mathematics in Biosciences and Medicine (CAMBAM). Funding from the Illawarra Cancer Carers and the PanCare Foundation (APP1165978, administered by Cancer Australia) awarded to KLV is also gratefully acknowledged. PSK was supported by the Australian Research Council Discovery Project (DP18010512). The funders had no role in study design, data collection and analysis, decision to publish, or preparation of the manuscript.

**Competing interests:** The authors have declared that no competing interests exist.

## Author summary

Pancreatic cancer has a dismal prognosis with a median survival of 3–5 months for untreated disease. The treatment of pancreatic cancer is challenging due to the dense nature of pancreatic tumours which impedes retention of drug at the tumour site. As such, systemic administration of chemotherapies, such as gemcitabine, has a limited efficacy. To overcome this, sustained-release devices have been proposed. These devices are injected locally and release drug over time, providing a concentrated local, sustained drug concentration. To investigate the possible efficacy of these devices, we developed a mathematical model that would allow us to probe treatment perturbations *in silico*. We modelled the individual cancer cells and their growth and death from gemcitabine loaded into the sustained delivery devices. Our platform allows future investigations for these devices to be run *in silico* so that we may better understand the forms of the drug release-profile that are necessary for optimal treatment.

## Introduction

Inoperable pancreatic ductal adenocarcinoma (PDAC) has a dismal prognosis, with a median survival of 3–5 months for untreated disease [1]. Treatment of PDAC with the chemotherapeutic agent gemcitabine can achieve clinical benefit and symptom improvement in 20–30% of patients [1,2], although PDAC is still regarded as a chemotherapy-resistant tumour [3,4]. Gemcitabine is designed to target and kill cancer cells by incorporating into the DNA strand of a PDAC cell allowing only one deoxynucleotide to be incorporated, which prevents strand elongation [5,6], resulting in cell cycle arrest and subsequent cell death [7,8]. Despite gemcitabine being established as a standard treatment for advanced PDAC over 20 years, most subsequent large phase III studies have not shown significantly improved survival benefit [9]. Overall prognosis for PDAC has seen little improvement in the last 3 decades, largely due to drug resistance and poor intratumoural drug accumulation.

The majority of chemotherapeutics, gemcitabine included, are administered systemically via bolus or infusion intravenous administration. This often results in significant systemic toxicity, with only a fraction of the injected dose reaching the tumour. As such, there has been a growing interest in the development of localised targeted delivery systems which can modify the bio-distribution of drugs and achieve local drug accumulation in the tumour tissue [10–12] (Fig 1). For example, drug-eluting polymeric implants are designed to deliver high concentrations of chemotherapeutic drugs directly at the tumour site over some period of time, overcoming transport and tissue barriers as well as limiting off-target toxicities [13]. Biodegradable implants, can be designed to provide sustained drug release over weeks or months, avoiding repeated external drug dosing, clinic visits and other surgical interventions. The characteristics of these devices make local delivery especially attractive for chemotherapeutics with a narrow therapeutic window or short *in vivo* half-life [14], such as gemcitabine. However, there is still some discussion around the optimal way in which the implanted devices should release drug, for example whether the rate at which drug leaves the device is variable or fixed.

Drug-loaded polymeric fibres can be prepared by various cross-linking methods and allow for drug molecules to be released in a controlled manner depending on the cross-linking type and methods [15]. Previously, Wade *et al.* [14] showed that wet-spun gemcitabine-loaded alginate fibres inhibited *ex vivo* PDAC spheroid growth and reduced PDAC cell viability compared to gemcitabine delivered as a free drug. In a subsequent study, Wade *et al.* [13,16] showed that a coaxial fibre formulation, in which the alginate was encased by a

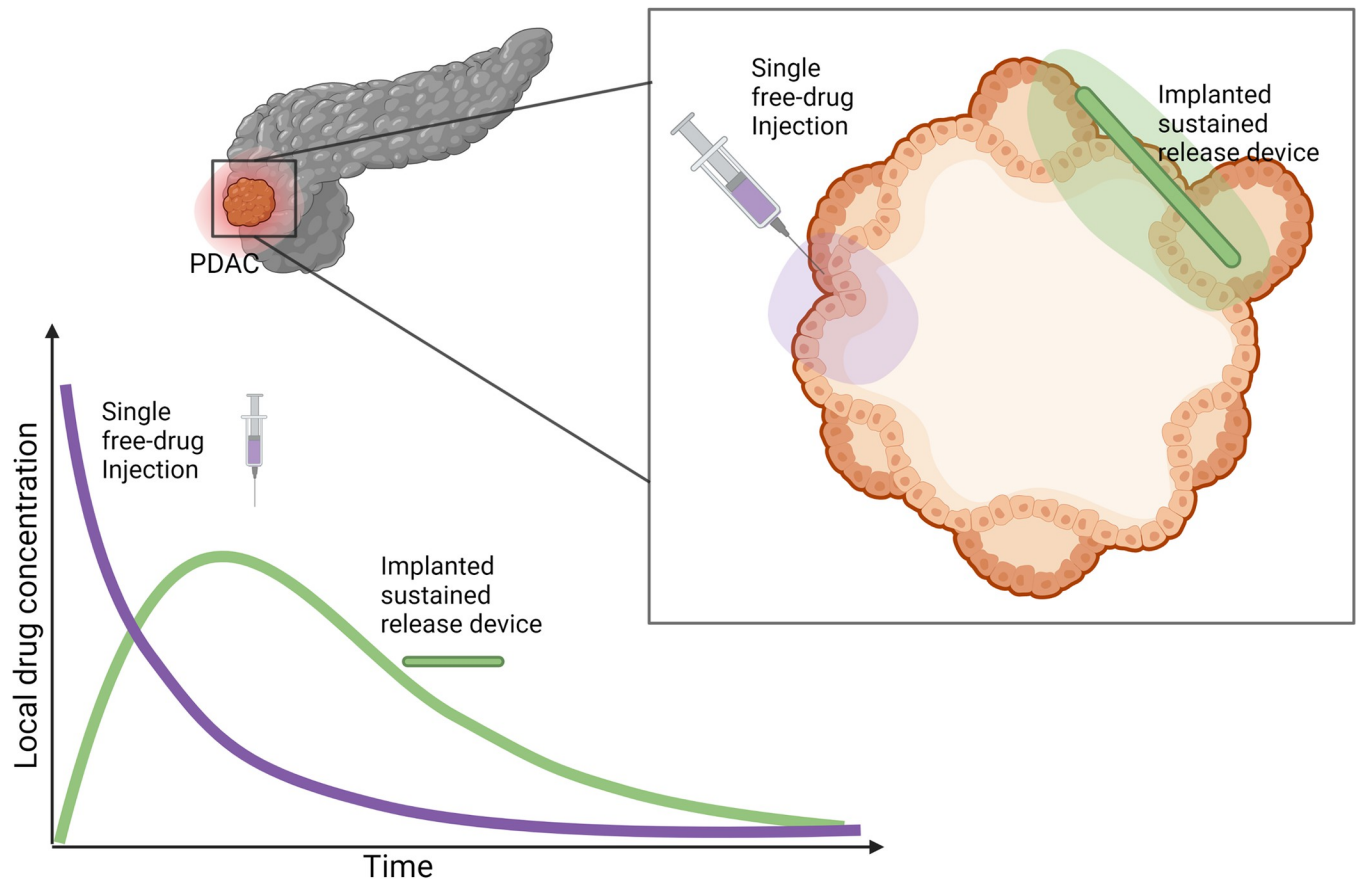


**Fig 1. Motivation for sustained-delivery implants for treatment of PDAC.** Sustained-delivery implants are a promising treatment methodology over conventional single free-drug intravenous or intratumoural injections. A hypothetical comparison of drug concentrations at the tumour site under these two protocols is pictured. Systemic injections of anti-cancer drugs often result in only a fraction of the drug arriving at the tumour site followed by a rapid decrease of drug concentration at the tumour site. In comparison, sustained-release mechanisms deliver drug over a prolonged period resulting in a durable drug presence at the tumour site. Created using biorender.com.

<https://doi.org/10.1371/journal.pcbi.1010104.g001>

polycaprolactone (PCL) shell, demonstrated significant *in vivo* antitumour efficacy; however, it is not possible to conclude experimentally whether an alternative release-profile of gemcitabine may be more effective. Fortunately, computational and mathematical modelling is well situated as a predictive tool for quantifying the efficacy of alternative drug release profiles and drug administration patterns.

Mathematical models have been used to help understand formation and treatment of a range of different cancers for some time now [17–22]. In particular, agent-based models (ABM) have been used extensively in cancer modelling as they allow for the consideration of spatial and phenotypic heterogeneity [23–31] which are known to be major drivers of variations in treatment outcomes. In ABMs, the likelihood of events, such as cell proliferation, movement, death or mutation are modelled as probabilities, allowing the simulation to evolve stochastically in time. ABMs have been used to contribute understanding to tumour growth dynamics [24,26–28], such as angiogenesis [31] and cell cycling [32]; the impacts of certain treatments [30,33,34]; and the likelihood of tumour recurrence [23]. ABMs have also been used to model chemotherapy treatment and movement through a tumour [35–41]. For example, Tang *et al.* [38] developed a 3D computational model of tumour growth under treatment with chemotherapy, where cells are modelled as discrete agents whose proliferation is

dependent on interstitial pressure and chemotherapy is captured by a partial differential equation (PDE). With their model they investigated the effects of the tumour microenvironment on the intratumoural distribution of chemotherapy and concluded that the main driver was the pressure difference within capillary blood and extracellular space. While important for intravenously administered chemotherapy, their model is too complex for considering an implanted degradable chemotherapy device. Furthermore, there is yet to be developed an ABM for the release of chemotherapy treatment through sustained-release or degradable devices. Insights on therapeutic failure in immunotherapy and virotherapy have also been provided through an ABM software known as PhysiCell [42–45]. There have been ABMs developed that specifically focus on pancreatic cancer growth [46,47]; however, an ABM describing pancreatic cancer growth and treatment with a degradable polymer implant has not yet been developed.

For some time, mathematical models of degradable drug delivery mechanisms have been used to assist in the understanding of polymer degradation, hydrolysis kinetics and the subsequent effect of drug release on the applied system [10,48–55]. Using mass-balance kinetic equations, McGinty *et al.* [52] investigated the extent to which variable porosity drug-eluting coatings can provide better control over drug release using transport diffusion equations. Their results indicate that the contrast in properties of two layers can be used as a means of better controlling the release, and that the quantity of drug delivered in early stages can be modulated by varying the initial drug distribution. More recently, Spiridonova *et al.* [56] fitted drug release from polymer microparticles and investigated the effect of size distribution on diffusional drug release from sustained-delivery systems using a system of PDEs. Whilst useful for capturing the drug delivery mechanism, most models of drug-loaded polymers such as these have not examined the influence of changes to drug release profiles on antitumour efficacy or how intratumoural stochasticity impacts drug delivery.

In this work, we have developed a hybrid mathematical and computational model of PDAC tumour growth and death from treatment with gemcitabine released from a polymeric fibre. We extended a previously published ABM known as a Voronoi cell-based model (VCBM) [57] to model tumour cell growth and death and coupled this with a PDE model for gemcitabine release from polymeric implants. *In vitro* drug release curves were used to optimise the PDE formulation describing how gemcitabine is released from fibres. A numerical simulation was then used to initialise the parameters in the ABM using *in vivo* control PDAC tumour growth measurements. The potential impact of these fibres on tumour growth and cell death was then investigated with the VCBM-PDE model and improvements on drug release kinetics and fibre placement were suggested. We quantified the impact of varying sustained-release profiles including a constant release, exponential release, and sigmoidal release from these devices. In this way, we could conclude whether the rate at which drug was released from the implant had any impact on treatment effectiveness. The model was developed as a tool that can be applied to interrogate other cancer therapies using polymeric implants with the goal to improve treatment response for PDAC patients.

## Experimental methods

**Ethics statement.** All animal experiments were conducted in accordance with the NHMRC Australian Code for the Care and Use of Animals for Scientific Purposes, which requires 3R compliance (replacement, reduction and refinement) at all stages of animal care and use, and the approval of the Animal Ethics Committee of the University of Wollongong (Australia) under protocol AE18/13.

**Fibre fabrication and characterisation.** Full details for the fabrication and characterisation of alginate fibres loaded with or without gemcitabine are described in Wade *et al.* [13,14].

Briefly, gemcitabine-loaded alginate fibres had a uniform surface area from 50–120  $\mu\text{m}$  in diameter. Experimentally, fibres displayed different drug release profiles and total drug released depending on the concentration of polymer used. Primarily, the effect of changing the alginate percentage and PCL presence was seen in the speed of release of the drug and time to full drug release; see [14] for more details. To investigate this further in this work, using a computational model we consider alternative release profiles not yet fabricated to examine their effectiveness, these include constant, exponential and sigmoidal release gradients. These are considered purely *in silico*. Fibre diameter also varied depending on the materials used [14].

**Fibre gemcitabine release kinetics.** Full details for the experiments measuring gemcitabine release can be found in Wade *et al.* [14] with brief details here. Gemcitabine-loaded fibres were added to 2mL of simulated body fluid (SBF), Ph 7.4 and incubated at 37°C. At various time points (10, 30, 60, 90 min hourly for 10h and then daily for 3 weeks), buffer solution (200 $\mu\text{L}$ ) was removed for analysis of gemcitabine release and replaced with fresh SBF. The amount of drug released from alginate fibres was determined using high performance liquid chromatography (HPLC). The amount of gemcitabine released ( $\mu\text{g}$ ) was calculated by interpolating AUC values from the standard curve using Empower Pro V2 (Waters) software.

**Implant toxicity *in vitro*.** Gemcitabine loaded fibres were tested for their cytotoxicity against human pancreatic cancer cells (Mia-PaCa-2) cells over 72h. Cells were incubated with 0.5 cm lengths of gemcitabine loaded or non-drug loaded fibre formulation before an endpoint MTS cell viability assay was performed. Results are displayed as a percentage of an untreated control. Experiments were performed in triplicate. Full details for the toxicity experiments can be found in Wade *et al.* [13].

***In vivo* Mia-PaCa-2 cell growth.** Animals were subcutaneously inoculated with 100 $\mu\text{L}$  suspension of  $1 \times 10^6$  Mia-PaCa-2 cells in PBS. Tumour volume measurements began when tumours reached a volume of 200  $\text{mm}^3$  using

$$\text{volume} = \text{width} \times \frac{\text{length}^2}{2}$$

where width is the longest tumour diameter measurement and length is the tumour measurement along the axis perpendicular to this (Fig H in S1 Text). Tumour volume was measured daily for a duration of approximately 33 days. Full details for this experiment can be found in Wade *et al.* [13]. All animal experiments were conducted in accordance with the National Health and Medical Research Council (NHMRC) Australian Code for the Care and Use of Animals for Scientific Purposes, which requires 3R compliance (replacement, reduction, and refinement) at all stages of animal care and use, and the approval of the Animal Ethics Committee of the University of Wollongong (Australia) under protocol AE18/13.

## Mathematical methods

The model developed for the release of gemcitabine from alginate fibres and the impact on a growing PDAC tumour is formulated in two parts below. The first describes the PDE describing the concentration of gemcitabine in the tumour microenvironment (TME) and surrounding tissue over time. The second describes the VCBM [57] that captures the way tumour cells proliferate, move and undergo apoptosis from gemcitabine. We chose to model the tumour growth and treatment in 2 dimensions as the *in vivo* tumour growth measurements were taken as only width and height measurements and we assumed any third-dimension effects were analogous to what happens in 2 dimensions. All parameters introduced for the model are summarised in Tables A-E in S1 Text and a schematic for the model is in Fig 2.

**Model of gemcitabine.** To capture the concentration of gemcitabine in the tumour microenvironment, we first considered a 2D rectangular domain with boundary  $B$  (Fig A in S1 Technical Supplementary Information). Inside this domain, is implanted a gemcitabine drug-loaded fibre which is represented by a vertical line source (panel A of Fig A in S1 Technical Supplementary Information and Fig 2A). Gemcitabine diffuses from the line source at some time-dependent rate that decreases as the polymeric fibre degradation slows. The

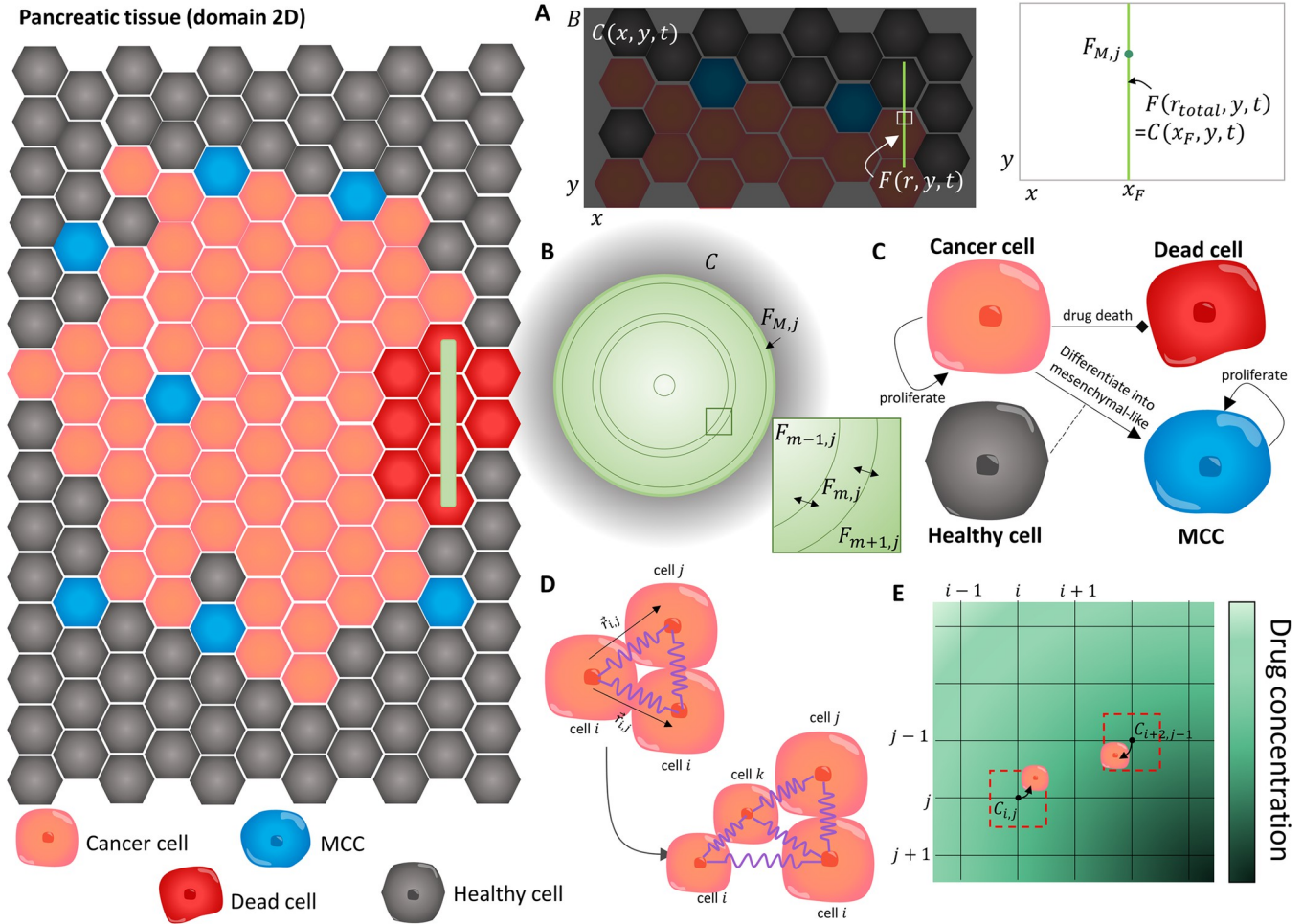


**Fig 2. The main components of the VCBM-PDE model.** In the VCBM, we model the interactions between healthy cells (grey), cancer cells (orange), MCC (blue) and dead cells (red) in a 2-dimensional tumour microenvironment cross section. (A) The concentration of drug in the TME was modelled in a 2 dimensional domain bounded by  $B$ , where  $C(x,y,t)$  was the concentration in the TME at position  $(x,y)$ . The fibre implant was then placed at a position  $x = x_F$  and modelled as a line source. To capture the diffusion of drug from the fibre, we modelled the concentration of gemcitabine inside the fibre  $F(r,y,t)$  at radial position  $r$  and domain position  $y$  where the continuity condition in Eq (3) required equal concentrations at the fibre boundary and at the immediate local microenvironment, i.e.  $F(r_{total},y,t) = C(x_F,y,t)$ . (B) The concentration of gemcitabine inside the polymeric fibres was modelled by radially symmetric diffusion Eq (2) using a finite volume method (FVM) discretisation and considering the 2D cylindrical cross section of the fibres which have length  $L$  and radius  $r_{total}$ . The fibre was discretised into concentric annuli  $F_{m,j}$  at annulus  $m$  and cross section  $j$ , ( $i = 0,1, \dots, M$ ) and the concentration of drug in each annulus  $F_{m,j}$  was modelled by considering drug diffusion across the boundaries (e.g.  $F_{m-1,j}$  and  $F_{m+1,j}$  flow into  $F_{m,j}$  and vice versa). The full discretisation is presented in S1 Technical Supplementary Information. (C) Modelling assumptions for the VCBM were that cancer cells (orange) proliferate and some are able to cause epithelial to mesenchymal transition and become invasive. We model this transition by assuming cells differentiate into a mesenchymal cancer cell (MCC) with one daughter cell placed on a neighbouring healthy cell. These MCCs cause the break down of surrounding tissue (i.e. replace healthy neighbouring cells with their progeny). Cancer cells can then die through gemcitabine uptake from their local environment. For more details see Fig B in S1 Text. (D) Individual cells were modelled as cell centres connected by springs [57]. The proliferation of a cell introduced a new cell into the lattice network which caused the rearrangement of the cells in the lattice with movement governed by Hooke's law. (E) To simulate the gemcitabine concentration in the TME, Eq (1), we introduced a FVM discretisation, where the gemcitabine concentration was defined at discrete volumes centered around points in the discretisation. Cells could take up drug from the nearest grid point to their centre, and this concentration was used to determine their likelihood of drug-induced cell-death.

<https://doi.org/10.1371/journal.pcbi.1010104.g002>

gemcitabine concentration in the domain outside the fibre is diffusing and decaying. PDAC cells in the domain are also taking up gemcitabine, removing it from the concentration in the domain. Inside the fibre, we model the diffusion of drug as radially symmetric (Fig 2B).

We denote the concentration of drug in the TME at position  $(x,y)$  by  $C(x,y,t)$  and model this concentration by

$$\frac{\partial C}{\partial t} = \overbrace{D\nabla^2 C}^{\text{diffusion}} - \overbrace{\lambda C}^{\text{decay}} - \overbrace{\sum_{\text{cells } i} \delta(x - x_i)\delta(y - y_i)v_c W_i C}^{\text{cell uptake}} + \overbrace{\delta(x - x_F)J(y, t)}^{\text{fibre release}}, \tag{1}$$

where  $D$  is the diffusion coefficient in the TME, and  $\lambda$  is the decay rate of the drug. To model cancer cells taking up gemcitabine, we used  $\delta(x)$  which is the Dirac delta function in one-dimension, where  $(x_i, y_i)$  is the  $i$ th cancer cell’s Voronoi centre position in the domain (Fig A in S1 Text), and  $W_i$  is the cell’s volume. Pancreatic cancer cells take up drug in the domain at a rate  $v_c$ . Cell uptake was modelled by point sinks analogous to that in PhysiCell and BioFVM [43,58], where cells are considered discrete “point masses” in the domain that take up drug from a single rectangular discretised voxel weighted by the local concentration of drug. We then used a line source at  $x = x_F, y_0 \leq y \leq y_0 + L$  to model the release of gemcitabine from the polymeric fibre, where  $y_0$  is the location of the bottom of the fibre and  $L$  is the fibre length (Fig B in S1 Technical Supplementary Information). This line source was represented by a Dirac delta function in one-dimension and the drug diffuses from the line source with flux  $J(y,t)$ .

To derive the flux of drug from the line source, we first assumed that the release of drug from the fibre would be time dependent. As such, we chose to explicitly model a concentration of drug diffusing inside the fibre. We denote the concentration of gemcitabine at radial position  $r$  and location  $(x_F, y)$  by  $F(r,y,t)$  (Fig B in S1 Technical Supplementary Information and Fig 2A). We model the diffusion and movement of drug inside the fibre assuming radial symmetry. We assumed that diffusion in the radial direction is significantly faster than along the fibre since the radius of the fibre  $r_{total}$  is significantly less than the length of the fibre  $L$  (Figs A and B in S1 Technical Supplementary Information). This gives

$$\frac{\partial F}{\partial t} = D_F(t) \frac{1}{r} \frac{\partial}{\partial r} \left( r \frac{\partial F}{\partial r} \right), \tag{2}$$

where  $D_F(t)$  is the time-dependent diffusion of drug inside the fibre. We imposed the continuity condition

$$F(r_{total}, y, t) = C(x_F, y, t), \tag{3}$$

so that the diffusion of drug out of the fibre at the line source will depend on the location  $(x_F, y)$  and local exterior concentration. The flux out of the line source  $J(y,t)$  in Eq (1) can then be approximated from the release of drug across the boundary of the fibre:

$$J(y, t) = \begin{cases} -\frac{2\pi r_{total}}{h} D_F(t) \frac{\partial F}{\partial r}(r_{total}, y, t) & y_0 \leq y \leq y_0 + L \\ 0 & y < y_0, y > y_0 + L \end{cases}. \tag{4}$$

This term is derived by converting the flux out of the radial fibre into the flux represented by the line source in Eq (1) and converting to a concentration per surface area where  $h$  is the depth of the rectangular region (presumed thin, see Fig A in S1 Technical Supplementary Information). Both Eq (3) and Eq (4) are necessary boundary conditions for Eq (1) and Eq (2). In this way, we assume the concentration is continuous and the flux of the fibre is equal to the flux into the TME, equivalent to a conservation of mass.

The diffusivity of the drug,  $D_F(t)$ , is modeled by the function

$$D_F(t) = \frac{k}{t + \epsilon} + D_{const}, \quad (5)$$

where  $k$  controls the gradient of the drug release rate (i.e. how quickly the fibre swells),  $D_{const}$  is the constant decay rate from the fibre and  $\epsilon$  is a tuning constant to provide a finite initial diffusion coefficient, i.e.  $D_F(0) = k/\epsilon + D_{const}$ . We expect  $D_F(0)$  to be initially large ( $>1$ ) since the polymeric fibre is hydrophilic and drug would immediately diffuse out of the fibre. In addition, some drug is never properly loaded into the fibre and can be released instantaneously. The formalism in Eq (5) was broadly chosen to capture the rapid decline in release as the polymeric fibre degrades. It is possible to model the breakdown of the drug release mechanisms to include device swelling and degradation and for examples of this see [56,59–61].

No-flux boundary conditions on  $B$ , the exterior of the TME, are imposed:

$$\frac{\partial C}{\partial \vec{n}} = 0$$

where  $\vec{n}$  is the outward unit normal on the boundary  $B$  (Fig E in S1 Technical Supplementary Information). In the case of a fibre implantation, all drug in the domain is initially situated in the fibre:

$$F(r, y, 0) = \frac{C_0}{\pi r_{total}^2 L}, C(x, y, 0) = 0, \quad (6)$$

where  $C_0$  is the amount of drug in  $\mu\text{g}$ , the denominator is the volume of the fibre and there is no drug initially in the domain  $B$ . We assume the location of the fibre is fixed in space over the course of the simulation and is not affected by cells around it. For more details on the derivation of the model see S1 Technical Supplementary Information.

We solved Eqs (1)–(4) numerically using a Finite Volume approximation. In particular, the diffusion of drug within the fibre, Eq (2), was solved through discretising the cross section of a fibre into annuli (see Fig 2B and S1 Technical Supplementary Information). The model is solved using a finite volume method (FVM) discretisation, for examples of this form of discretisation in cancer growth and treatment see [62–70]. As part of the investigations of these fibres in this work, we chose to quantify the impact of varying the drug release profile to a constant release, exponential release, or sigmoidal release profiles. To do this, we replaced the drug diffusion in Eq (2) by the corresponding profile being examined and imposed drug conservation on the total drug released. More details on this can be found in S1 Technical Supplementary Information.

**Voronoi Cell-Based Model (VCBM) of pancreatic tumour growth.** Agent-based models (ABMs) are primarily used to simulate heterogeneity that arises through stochasticity in cellular interactions. We present an ABM to capture the 2D formation of a pancreatic tumour in the pancreas. Our model extends a Voronoi cell-based model (VCBM) for tumour growth already published in [57]. The model describes how individual cells behave over time by considering their behaviour to be a stochastic process. We consider a set of  $(x, y)$  points in the domain  $B$  as representatives of cell centres and then overlay this with a Voronoi tessellation to define individual cell boundaries. A Voronoi tessellation defines the region of space where the Euclidean distance to a point is less than the distance to any other point  $e$  in the lattice. Voronoi tessellations have been used to model tissue and cancer cell dynamics for some time [71–75]. Using a Voronoi tessellation for the ABM allows cell morphology to be heterogeneous and not fixed, and the morphology can change with cell movement. The model is solved on a time increment of 1hr to account for the fact that cellular interactions are slow in comparison to



drug diffusion (**Fig C in S1 Technical Supplementary Information**). To model pancreatic tumour formation, we assumed the primary functions of pancreatic tumour cells were movement and proliferation. Below are details of the cell types, the model for cell movement and proliferation, a description of the dynamics of tumour mesenchymal cells, the model for cell death and details of how the domain changes as the tumour grows.

PDAC cells can acquire mesenchymal-like phenotype properties through a process known as epithelial-mesenchymal transition (EMT) [76–79]. In the EMT process, epithelial elements undergo cytoskeleton remodelling and migratory capacity acquisition due to the loss of intracellular contacts and polarity [77]. This enables the formation of mesenchymal-like cancer cells (MCCs) which have enhanced migratory capacities and invasiveness, as well as elevated resistance to apoptosis [78]. Since there is evidence that EMT plays an important role in PDAC progression [76–79], we have introduced this cell type into the model.

We considered four main cell types in the model: healthy pancreatic cells, PDAC cells, MCCs and dead cells (cancer cells that have experienced drug-induced death); see **Fig 2C**. Each cell has an initial location in domain  $B$  such that for cell  $i$  its cell centre would be at  $\vec{r}_i = (x_i, y_i)$ . The initial tissue comprises of healthy cells, arranged so that the corresponding Voronoi cells form a hexagonal tessellation, analogous to other work in the literature [80,81]. To initialise the tumour formation, we removed a healthy cell from the centre of the domain and replaced it with a pancreatic tumour cell (**Fig A in S1 Text**). These pancreatic tumour cells could proliferate, die from gemcitabine, or form MCCs. Once formed, these MCCs then move and proliferate until they die. Healthy cells are assumed to be able to move or be removed from the domain by being replaced by MCCs (**Fig B in S1 Text**).

Cell movement is governed by pressure-driven motility, modelled using Hooke’s law [57]. Each cell’s  $(x,y)$  position is updated by calculating the effective displacement of the cell’s lattice point by the sum of the forces exerted on that cell, where force is modelled as a network of damped springs connecting a cell to its nearest neighbours (defined by a Delaunay triangulation). To determine the movement of an individual cell, we use the vector representation for that cell’s  $(x,y)$  position from the origin  $\vec{r}_i = (x_i, y_i)$ . For cell  $i$ , the displacement of this point in time  $\Delta t_{cells}$  is given by

$$\vec{r}_i(t + \Delta t_{cells}) = \vec{r}_i(t) + \lambda_m \sum_{vj} \frac{\vec{r}_{ij}(t)}{\|\vec{r}_{ij}(t)\|} (s_{ij}(t) - \|\vec{r}_{ij}(t)\|), \tag{7}$$

where  $\vec{r}_i(t)$  is the vector representation for the  $i$ th cell’s centre position in the lattice at time  $t$ ,  $\lambda_m$  is a damping and mobility constant,  $\vec{r}_{ij}$  is the vector between cell  $i$  and  $j$ ,  $s_{ij}$  is the spring rest length (equilibrium distance) between cell  $i$  and  $j$ . Cells  $j$  are the cells connected to cell  $i$  in a Delaunay triangulation, i.e. in a neighbourhood of cell  $i$ . The introduction of new cells in the lattice through proliferation introduces new spring connections and shortens or extends others, promoting the movement of cells in the environment (**Fig 2D**).

Tumour cell proliferation was assumed to be a function of the cell’s distance,  $d_{neut}$  to the nutrient source (tumour periphery, i.e. nearest healthy cell centre, see **Fig C in S1 Text**). The maximum radial distance for nutrient-dependent cell proliferation is  $d_{max}$ . Cells that are a further distance from the nutrients than  $d_{max}$  enter a quiescent (non-proliferative state), forming what is commonly known as a necrotic core. The probability of a cell dividing  $p_d$  in time step  $\Delta t_{cells}$  is given by

$$p_d = \begin{cases} p_0 \left(1 - \frac{d_{neut}}{d_{max}}\right) & d_{neut} \leq d_{max} \\ 0 & d_{neut} > d_{max} \end{cases}, \tag{8}$$

where  $p_0$  is a proliferation constant derived based on the maximum rate of cell proliferation  $\phi$  (i.e.  $p_0 = 1 - \exp(-\phi\Delta t_{\text{cells}}) \approx \phi\Delta t_{\text{cells}}$ ). The formalism in Eq (8) is similar to what was used by Kansal *et al.* [82], and Jiao and Tarquato [83].

Mechanical feedback between cells has been shown to be a regulatory mechanism for growth control of tissue cells *in vitro* and *in vivo* [84]. A cancer cell's ability to proliferate, while generally considered to be dysregulated, has been shown to slow down and eventually arrest with compression from neighbouring cells [85,86]. To model this, we introduced a constraint on cell proliferation: if all cells within a cell's neighbourhood (i.e. connected to that cell by a Delaunay triangulation) are within  $s/p_{\text{age}}$  of the cell, then the cell will not proliferate. If a cell  $i$  proliferates, a new lattice point  $j$  is created and the two cells are placed at a distance  $s/p_{\text{age}}$  from the original proliferating cells position at a rotation  $\theta \sim U(0,2\pi)$  (Fig 2D). To simulate the enlargement and repositioning of the daughter cells, the resting spring length of the connection between  $i$  and  $j$  linearly increases over time from  $s/p_{\text{age}}$  to the mature resting spring length  $s$  as was formulated in our previous work [57]; see Fig C in S1 Text. Once a cell has proliferated, it takes  $g_{\text{age}}$  time steps before the daughter cell will try to proliferate again, accounting for G1 phase of the cell cycle where the cell transitions from mitosis M to DNA synthesis S [57]. It is well known that tumours contain highly heterogeneous populations of cells that have distinct reproductive abilities. To account for heterogeneity in the cell cycling, cells sampled the age at birth from a Poisson distribution with mean 50.

MCCs are created at the boundary of the tumour with probability  $p_{\text{MCC}}$ . These cells are created from tumour cell differentiation. In this way, a single tumour cell can either proliferate into two new tumour cells or undergo differentiation into a tumour cell and an MCC. We model the invasive property of MCCs by placing the newly differentiated MCC daughter cell at the position of a neighbouring healthy cell, removing that healthy cell from the domain; see Fig B in S1 Text. As such, through their creation, these MCCs contribute to the degradation of the healthy tissue surrounding the tumour.

As in [87–90], we assumed that cancer cells die from gemcitabine contact at a rate described by the Michaelis-Menten term

$$\beta = \frac{\delta_m C_{i,j}}{C_{i,j} + IC_{50}},$$

where  $\delta_m$  is the maximum death rate due to the drug,  $C_{i,j}$  is the concentration of drug at the grid position  $(i,j)$  in the FVM discretisation closest to the cell's centre (Fig 2E and S1 Technical Supplementary Information), and  $IC_{50}$  is the concentration at which half the effect of the drug is attained. From this, the probability of an individual cell dying can be determined by assuming  $\text{Prob}(\text{cell death}) = 1 - \exp(-\beta\Delta t_{\text{cells}}) \approx \beta\Delta t_{\text{cells}}$ . While we chose not to model explicitly the resistance to gemcitabine that cancer cells can develop [3,4], we believe that by modelling cell death probabilistically we can capture some of the heterogeneity that may exist intratumourally. If a cell dies, then its phenotype changes to be a dead cell and it takes  $d_{\text{age}}$  hours to disintegrate. To simulate disintegration, at each time increment the spring rest lengths of a dead cell to each of its neighbours,  $s_{i,j}$ , decreases by  $s_{i,j}/d_{\text{age}}$ . Once the dead cell has disintegrated, it is removed from the simulation and the space left behind becomes "empty space" which is plotted in white. Cells are free to move into this space over time following Hooke's law.

As the tumour grows, the model domain expands. To reduce computational cost, new healthy cells are added to the domain only when a tumour cell's radial distance from empty space is  $<10$  model units (Fig D in S1 Text). A summary of the overall model rules is provided in a decision tree diagram in Fig E in S1 Text.

## Numerical simulations and parameter estimation

The VCBM-PDE model was written in C++ and simulations called through Matlab 2021b by creating a definition file for the C++ library using *clibgen* and *build* in Matlab 2021b. Code for the model at the various stages (e.g. fibre, single injections) can be found on github (<https://github.com/AdrienneJennerQUT/hybrid-VCBM-of-gemcitabine-and-pancreatic-cancer>).

Full details on all aspects of the code can be found in **S1 Code Documentation**.

An approximation for tumour volume was then determined from the 2D simulations using the same formula as the calibre measurements, multiplied by a scalar  $\sigma$ :

$$volume = width^2 \times \frac{length}{2} \times \sigma^3$$

where *width* is the longest distance of a cell on the periphery from the centre and *length* is the distance of the farthest cell from the centre on the radial axis perpendicular to the radial axis of the longest distance (**Fig H in S1 Text**) where  $\sigma$  unit length of the model is equivalent to 1 mm. This calculation choice was made to closely resemble the tumour volume calculation with calipers done *in vivo*. As the size of the computational domain was smaller than the size of the real tumour, the length unit was scaled by  $\sigma$ , which scaled the unit length in the VCBM domain to a comparable mm unit measurement that reduced the computational cost. We chose  $\sigma = 0.1728$ .

We performed a convergence test for the VCBM to determine a threshold for the minimum number of simulations of the model to have average convergence at day 33 (**Fig F in S1 Text**). We found that from 500 simulations onward, the average tumour volume at day 33 had converged to some mean value. As such, we picked  $n = 500$  to be the number of simulations of the model we would run at each investigation.

To fit the parameters in the model, we first consider only the drug release and diffusion compartment of the model and using *in vitro* fibre release data obtain the relevant parameters for this compartment. Following this, we fit the cell proliferation and death rates based on *in vitro* cell count and viability measurements. Lastly, we estimate the remaining VCBM cell proliferation parameters by using a Latin Hypercube Sampling (LHS).

All fitting was undertaken using *lsqnonlin* in Matlab 2021b using *pdepe* and *ode45* to simulate the model. Parameters in the model were fit using experimental data or estimated from the literature. To fit the parameters relating to drug release from the fibre we used the *in vitro* drug release experiments. We simplified the model to consider only one cross section, i.e.  $F_{m,j} = F_m$ , since the outside concentration of drug was independent of location in the absence of cells in the *in vitro* experiment.

To estimate parameters for the pancreatic cell growth kinetics, we did a large Latin Hypercube sample of the parameter space and determined parameters that resulted in a minimal least squares distance to the *in vivo* control tumour growth measurements. To do this, we set an initial seed and obtained 1000 samples of the parameter space and simulated the model 30 times for each sample each time calculating the residual between the data and the simulation. The parameter sample with the lowest average was then fixed for the remainder of the model simulations. It should be noted that this method does not provide us with a fitted parameter value but was a numerical way of obtaining a reliable estimate for these parameters. Other parameters were either fixed to previous values in the literature or estimated based on previous work. See **Tables A-E in S1 Text** for a full summary of all parameter values and relevant references.

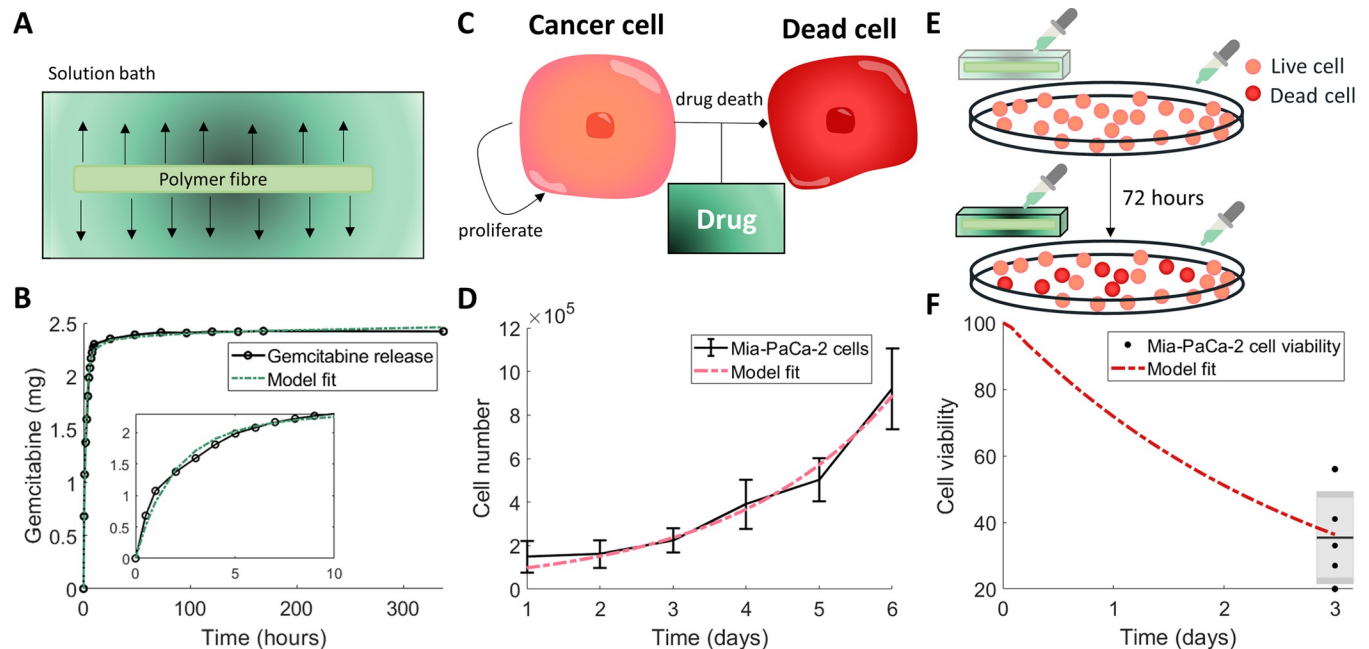


**Fig 3. Calibration of model parameters to in vitro experiments.** (A) Drug release profiles for gemcitabine with 3% alginate 15% PCL were measured by placing the gemcitabine-loaded alginate fibre in a solution bath and measuring the released drug concentration over time. (B) The drug concentration in the solution bath (black) was used to fit model parameters for the drug release from the fibre (green). Resulting parameters are in **Table A in S1 Text**. (C) The drug-induced death rate of pancreatic cancer cells was determined by simplifying the full model assumptions to consider a homogeneous model for live cancer cells  $P_L(t)$  that were proliferating and dying (become dead cells  $P_D(t)$ ) through the effect of the drug gemcitabine  $C(t)$ , **Eqs (9)–(11)**. (D) Fitting an exponential growth curve to Mia-PaCa-2 cell proliferation in vitro [91] gave the growth rate of cells  $\phi$ . Values are the mean  $\pm$  std. (E) To measure the efficacy of the protocol, the cell viability was determined after aliquots from drug released from gemcitabine-loaded fibre were placed in a well with proliferating Mia-PaCa-2 cells at 24, 48 and 72 hours. (F) The resulting cell viability at 72 hours from the experiment depicted in (E) was used to fit the drug-induced cell death rate (**Eqs (9)–(11)**). The data is plotted as a box and whisker plot. Resulting parameters for (D) and (F) are in **Table B in S1 Text**.

<https://doi.org/10.1371/journal.pcbi.1010104.g003>

## Results

### Calibration of drug release kinetics and drug-induced cell death to in vitro measurements

Gemcitabine-loaded fibres were placed in a solution bath and the resulting cumulative concentration of gemcitabine measured (**Fig 3A**). To obtain a model describing the release rate of the drug from the fibre, we fitted parameters from **Eqs (1)–(4)** to these *in vitro* measurements for the release of gemcitabine from 3% alginate 15% PCL fibres [14]. Fitting the release curve parameters  $k$ ,  $d_{const}$ ,  $C_0$  and  $A_{out}$  gave the fit in **Fig 3B** and parameter values in **Table A in S1 Text**. Overall, the model was able to obtain the fit to the data and followed the trend which showed a rapid initial release of gemcitabine followed by a steady-state threshold. We validated the model's predictive capability by also fitting gemcitabine release from 1% and 2% alginate fibres (**Fig G in S1 Text**).

To assess the efficacy of the drug on inducing death in PDAC cells, cell viability studies were performed using Mia-PaCa-2 cell lines. To model these experiments, we considered a simplified deterministic and spatially independent version of our model with only live cancer cells  $P_L(t)$ , dead cancer cells  $P_D(t)$  and a concentration of drug  $C(t)$ :

$$\frac{dP_L}{dt} = \phi P_C - \frac{\delta_m C}{C + IC_{50}} P_C, \quad (9)$$

$$\frac{dP_D}{dt} = \frac{\delta_m C}{C + IC_{50}} P_C, \quad (10)$$

$$\frac{dC}{dt} = \mu(t) - \lambda C, \quad (11)$$

where  $\phi$  is the exponential proliferation rate of cancer cells *in vitro*,  $\delta_m$  is the death rate of cancer cells by gemcitabine,  $IC_{50}$  is the drug's half effect concentration, and  $\lambda$  is the decay rate of the drug (Fig 3C). To first determine the proliferation rate of pancreatic cancer cells *in vitro*, an exponential growth curve was fit to cell count measurements for Mia-PaCa-2 cells [91] (Fig 3D, parameter values Table B in S1 Text) using simple exponential growth (i.e. setting  $C(0) = 0$  in Eq (9)). Fixing this growth rate and the estimate for the decay rate of drug, we then determined the antitumour efficacy of gemcitabine-loaded fibres in the cell viability experiments. Cells were treated with aliquots of simulated body fluid from gemcitabine-loaded fibres that had been incubating for 24, 48 or 72 h (Fig 3E). To simulate these experiments, the model is solved piecewise such that  $\mu(t) = \delta(t - t_{\text{aliquot}})C(t_{\text{aliquot}})$ , where  $t_{\text{aliquot}}$  are the times of the drug administrations. An approximation for the concentration of drug at each time point,  $C(t_{\text{aliquot}})$ , can be determined using the calibrated PDE model for drug release from the fibres. Fitting the drug-induced death rate and  $IC_{50}$  gave a good approximation to the data (Fig 3F). The resulting parameter values from the fit of the model can be found in Table B in S1 Text.

### Calibration and sensitivity of pancreatic tumour growth

The VCBM simulation of pancreatic tumour growth in the absence of treatment depicts invasive and disorganised movement of cancer cells into surrounding healthy tissue (Fig 4A). To calibrate tumour growth parameters in the model, we used an exhaustive numerical search of the parameter space using a Latin Hypercube Sampling for  $g_{\text{age}}$ ,  $d_{\text{max}}$ ,  $p_0$  and  $p_{\text{MCC}}$ , where we were minimising the least squares of the simulation with the *in vivo* tumour volume of Mia-PaCa-2 cells over 33 days (Fig 4B and Table C in S1 Text). To obtain an understanding of the stochasticity in our model, we fixed the parameter values obtained and we simulated the model 500 times and plotted the tumour volume over 33 days. From Fig 4B, while the growth is varied at points, there are no distinct outliers or unusual tumour growth rates, and the standard deviation throughout the entire period of observation remains small. In addition, the simulations sit within the *in vivo* tumour growth measurements from Wade *et al.* [13] for untreated pancreatic cancer growth. The histogram for the number of MCCs across the simulations (Fig 4C) shows only a small number of MCCs are created over the 33 days of growth, which is realistic when considering the ratio between a single cell agent in the model and a real cell in a biological tumour and matches findings that MCCs will compose only a small subset of the tumour [92–94].

To analyse the drivers of pancreatic tumour growth dynamics in our model, we conducted a detailed sensitivity analysis. A systematic multi-parameter sensitivity analysis was performed for  $\mathbf{p} = [p_0, p_{\text{MCC}}, d_{\text{max}}, g_{\text{age}}, p_{\text{age}}]$  using weighting identified by Wells *et al.* [95] (Fig 4D). This sensitivity analysis can identify combinatorial influences of multiple parameters and elucidate systemic features of the model. The average tumour volume predicted by the model at day 33 for 500 simulations was recorded for each parameter set. Pairs of parameters were varied, with each cell of Fig 4D depicting the weighting applied to each parameter in  $\mathbf{p}$  from 0.25, 0.75, 1.25, 1.75, and 2.25. This allowed for all combinations of alterations for two parameter values to be tested.

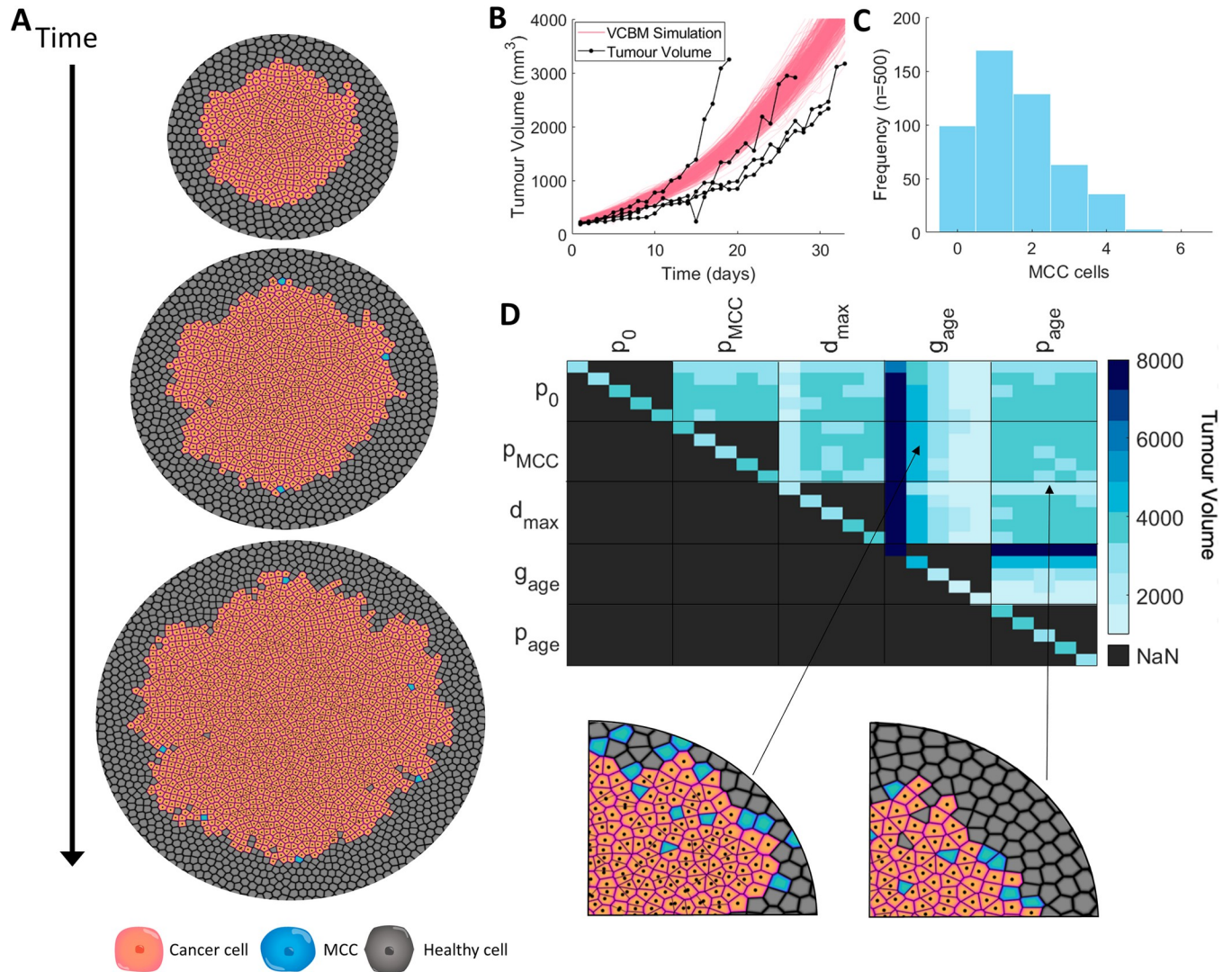


**Fig 4. Using the VCBM to model control tumour growth.** (A) Snapshots of the model simulation at 0, 5 and 10 days with cancer cells in orange, MCCs in blue and healthy cells in grey (a zoomed in version is in Fig I in S1 Text). (B) Mia-PaCa-2 tumour volume over 33 days measured in vivo in mice (black,  $n = 4$ ). Overlaid is the tumour volume from the VCBM simulation (pink,  $n = 500$ ) with parameters from Table C in S1 Text. (C) MCC counts in the VCBM simulations ( $n = 500$ ). (D) Sensitivity analysis of control tumour growth. Maximum tumour volume over 33 days for perturbations of parameters with weights of 0.25, 0.75, 1.25, 1.75 and 2.25, and spatial plots of large and small tumours simulated using the depicted weightings. In the heatmap, each pixel represents 500 averaged simulations with two parameters. In the boxes, the parameters vertically and horizontally in the grid are the weightings in ascending order, with each pixel being a “coordinate” representing the weighting for each parameter and the result from 500 averaged tests. Diagonal pixels only use individual parameters with different weightings. Legend for cell colouring: cancer cell (orange) healthy cell (grey), MCC (blue).

<https://doi.org/10.1371/journal.pcbi.1010104.g004>

The time taken for a cell to prepare for mitosis,  $g_{age}$ , has the greatest impact on final tumour volume (Fig 4D). Increasing  $g_{age}$  decreases tumour volume and conversely a decrease in  $g_{age}$  increases the final volume. As a result, the model predicts that if cells take longer to move through the cell cycle and undergo mitosis this will result in a smaller tumour volume. Reducing the maximum distance,  $d_{max}$ , from the periphery at which a cell can still proliferate decreases the final tumour volume. This is to be expected, as reducing the proliferating cell rim (through decreasing the distance from the periphery for which cells can proliferate) will reduce the number of cells available to proliferate and subsequently reduce the tumour volume. Decreasing the value of  $d_{max}$  only appears to have a significant impact on the final

tumour volume when the weighting applied is  $\leq 50\%$ . In comparison with  $d_{max}$  and  $g_{age}$ , the tumour volume is insensitive to changes in both the probability of a cell proliferating if it has reached mitosis,  $p_0$ , and the probability of a new pancreatic cancer stem cell being created,  $p_{MCC}$ . The time taken for a cell to reach adult size (when it can proliferate),  $g_{age}$ , similarly has a negligible impact on the tumour volume.

### Intratumoural implantation provide an alternate effective protocol

As previously shown by Wade *et al* [13–16], pancreatic cancer growth was inhibited under administration of gemcitabine as a free drug. This growth inhibition was furthered when gemcitabine was administered in loaded alginate fibres. Before quantifying the efficacy of varying gemcitabine-loaded fibre characteristics, we first looked to evaluate the impact of varying protocols for single point free-drug injections (Fig 1) of gemcitabine on the tumour volume. Simulating single point free-drug injections with the VCBM-PDE is a simplification of the full model presented in Eqs (1)–(4) where  $F(r,y,t) = 0$ . More details on this can be found in [S1 Technical Supplementary Information](#). We considered free-drug injections of gemcitabine as administered along a radial axis of the tumour in either a single dose or four free-drug injections which are rotationally symmetric (Fig 5A). In the case of the four injections, the total dosage is spread across the injections so that the total amount of drug administered is conserved.

Simulations of the model under the different injection protocols can be found in [Figs 5B and 5C](#), and [J in S1 Text](#). The sensitivity of parameter values governing tumour volume were again probed, now under a single administration of gemcitabine at the centre of the tumour ([Figs 5D and 5E](#), and [K in S1 Text](#)). The same trends with  $g_{age}$  and  $d_{max}$  were observed; however, an additional parameter, which represents the concentration the drug required to have an impact on the tumour volume,  $IC_{50}$ , was found to influence the volume under further perturbations of the parameter value ([Fig 5E](#)). As expected, a lower value of  $IC_{50}$ , which indicates that a smaller concentration of the drug is required for it to influence cancerous cells, leads to a lower tumour volume, while an increased value of  $IC_{50}$  leads to a higher tumour volume when compared to original estimate for  $IC_{50}$ .

To determine the effect of injection placement on tumour volume over time, we considered two protocols. The first was a single injection into the tumour of concentration  $C_0$ , and the second was four injections into the tumour, each of concentration  $C_0/4$  placed at equal rotations around the tumour. For each of these protocols we considered five potential placements of each injection at a distance  $d_m$  from the centre: a central injection ( $d_m = 0$ ), and injections  $d_m = 0.9$  mm from the centre,  $d_m = 1.7$  mm from the centre,  $d_m = 2.5$  mm from the centre and  $d_m = 3.5$  mm from the centre ([Fig 5A](#)). For example, for the second protocol where four injections are being placed, we could choose a distance  $d_m = 2.5$  mm from the centre of the tumour for the placement of the injections and the four injections were then placed at equal rotations around the tumour centre. For each of these placements, 500 simulations were run over 33 days and both the number of tumour cells and the tumour volume over time were measured ([Fig 5F](#)). For a single injection, distance did not impact the effectiveness of the injection and the tumour volume is qualitatively similar. The tumour volume was more significantly affected by distance in the case of four injections ([Fig 5F](#)), with free-drug injections further away from the centre of the tumour performing worse than those intratumoural injections. Primarily, single free-drug injections implanted peritumourally may encourage branching of external tumour structures in the model, and hence increase the calculated volume as it is based on the maximum distance from the centre of the tumour to the edge. Tumours with invasive edges or branching formations have been shown in some cases to be more challenging to treat in the long term [83,96]. From our model, this suggests that avoiding injection protocols that induce

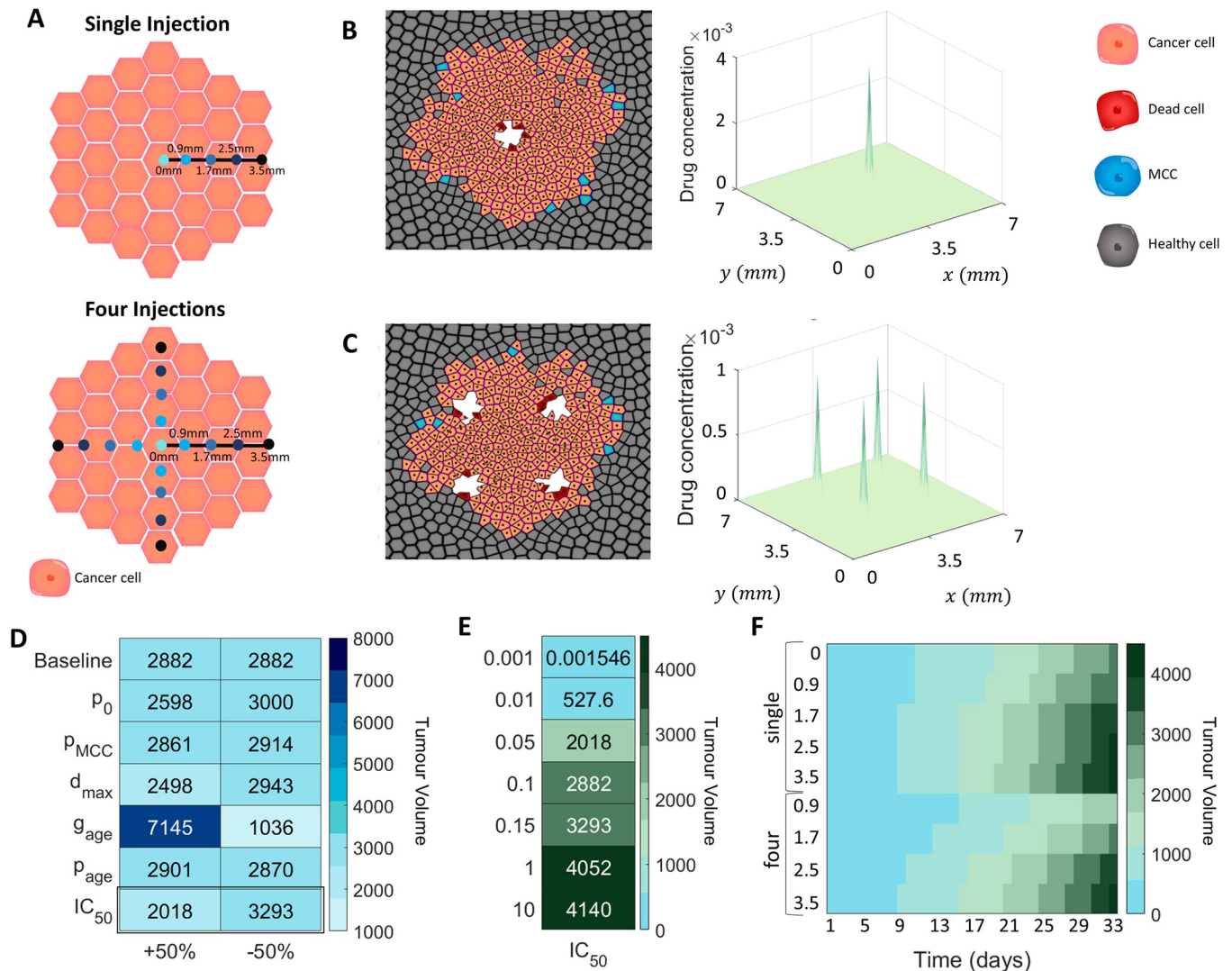


**Fig 5. Impact of intratumoural free-drug point injections on tumour cell eradication.** (A) Tumour growth was investigated under different gemcitabine single free-drug injections: central, 0.9 mm from centre, 1.7 mm from centre, 2.5 mm from centre, 3.5 mm from centre. Locations of injections on the tumour surface for a single free-drug injection or four free-drug injections is depicted schematically. (B) VCBM with a single central injection and the drug concentration at 24h. (C) The tumour volume with four injections placed  $30\mu m$  from the centre, and the drug concentration at each location at 6h. (D) Maximum tumour volume over 33 days for  $\pm 50\%$  perturbations in parameter values compared to the normal value (i.e. baseline parameter values). (E) Maximum tumour volume over 33 days for different perturbations of  $IC_{50}$  compared to the normal volume. (F) The tumour volume over 33 days with each injection protocol, averaged over 500 simulations. Legend for cell colouring: cancer cell (orange) healthy cell (grey), MCC (blue), dead cell (red). Note, the white space in the simulation images represents ‘empty space’ in the tumour where dead cells have been previously, but have since disintegrated.

<https://doi.org/10.1371/journal.pcbi.1010104.g005>

branching is crucial. While we present an approximation for tumour volume and placement of injections in units relevant to *in vivo* models (i.e.  $mm^3$  and mm respectively), more work needs to be done to validate that the efficacy of treatment predicted by the model would map to the human scale.

### Fibre location and release kinetics are a major driver of tumour arrest or tumour growth

Using the VCBM-PDE, we analysed the impact of varying the position of the fibre and the initial drug concentration on the tumour growth dynamics (Fig 6A). We introduced three



classifications for the tumour growth dynamics: tumour eradication (i.e. a tumour volume  $< 1\text{mm}^3$ ) tumour stabilisation, i.e. a tumour volume at day 33 less than the initial tumour size ( $\approx 100\text{mm}^3$ ), and tumour growth, i.e. a tumour volume on day 33 greater than the initial tumour volume. Large concentrations of gemcitabine loaded into the fibre positioned at  $d_m = 3.5\text{ mm}$  or  $d_m = 4.3\text{ mm}$  from the tumour centre were unable to stabilise or eradicate the tumour, also known as tumour arrest (Figs 6B and 6C, and M in S1 Text). Once the fibre was positioned closer to the tumour centre ( $\leq 1.7\text{ mm}$ ) lower concentrations of drug were sufficient to result in stabilisation of the tumour growth (Fig 6B). It was only with high drug concentration and centered fibres that we saw complete tumour eradication (Fig L in S1 Text). There are large variations in the response of tumour growth to the different protocols, suggesting that tumour stabilisation or arrest might be achievable for some tumours whereas others might experience tumour growth even in the presence of drug-loaded fibre.

To then analyse the effects of changes to the drug release profile on the tumour growth, we investigated four different release profiles: constant release, exponential release, sigmoidal Emax/Imax release profiles [97–99] (See Section TS3 in S1 Technical Supplementary Information). Each of these release profiles were parameterised by a release rate  $\gamma$  and for the Emax and Imax curves a half-effect term  $\eta$ . The different release profiles were tested with the fibre placed either centrally (intratumourally) (Fig 6D) or on the periphery of the tumour (peritumourally) (Fig 6E). The four different release profiles (constant, exponential, sigmoid emax, sigmoid imax) were tested with 8 different release rates. For each parameter value, 500 simulations were run over 33 days, with an initial amount of  $500\text{ }\mu\text{g}$  of gemcitabine.

For fibres positioned in the centre (Fig 6D), it is possible to eradicate the tumour with all release profiles considered given a small enough value of  $\gamma$ . In comparison, none of the drug release profiles resulted in tumour eradication when positioned peripherally (Fig 6E). Although, of note, the exponential release profile performed best out of the four release cases in both the centered and peripheral fibre configurations. Overall, the results suggest that it is possible to reduce tumour size with peripheral fibre injections irrespective of the shape of the release curve.

## Discussion

PDAC is a difficult-to-treat cancer with a poor prognosis. Novel therapeutic interventions are desperately needed to improve patient survival. While chemotherapy drugs, such as gemcitabine, have shown durable efficacy for pancreatic cancer, there has been little to no improvement in patient survival in the last 30 years [100]. PDACs are notorious for a dense fibrotic stroma that is interlaced with ECM [101] and is a major cause of therapeutic resistance [102]. One way of improving drug retention at the tumour site, and by consequence increase tumour eradication and patient survival, is through sustained-delivery devices (Fig 1). Polymeric fibres loaded with gemcitabine have shown increased therapeutic efficacy over conventional treatment delivery. To further analyse the potential of these novel therapeutic implants, we have designed a hybrid Voronoi cell-based model (VCBM)-partial differential equation (PDE) model to describe pancreatic tumour formation in healthy pancreatic tissue and the resulting effect of gemcitabine on the tumour tissue when delivered locally. With this model, we considered both the impact of a single fibre implanted with varying drug release profiles and hypothesised alternative and more effective treatment protocols.

The model was calibrated to *in vitro* and *in vivo* data. A limitation of this calibration was the lack of spatial data available to calibrate the parameters in the model. To try and quantify the impact of this limitation we performed a range of sensitivity analyses at different stages of the model investigation. The parameter sensitivity analysis then revealed that the fundamental

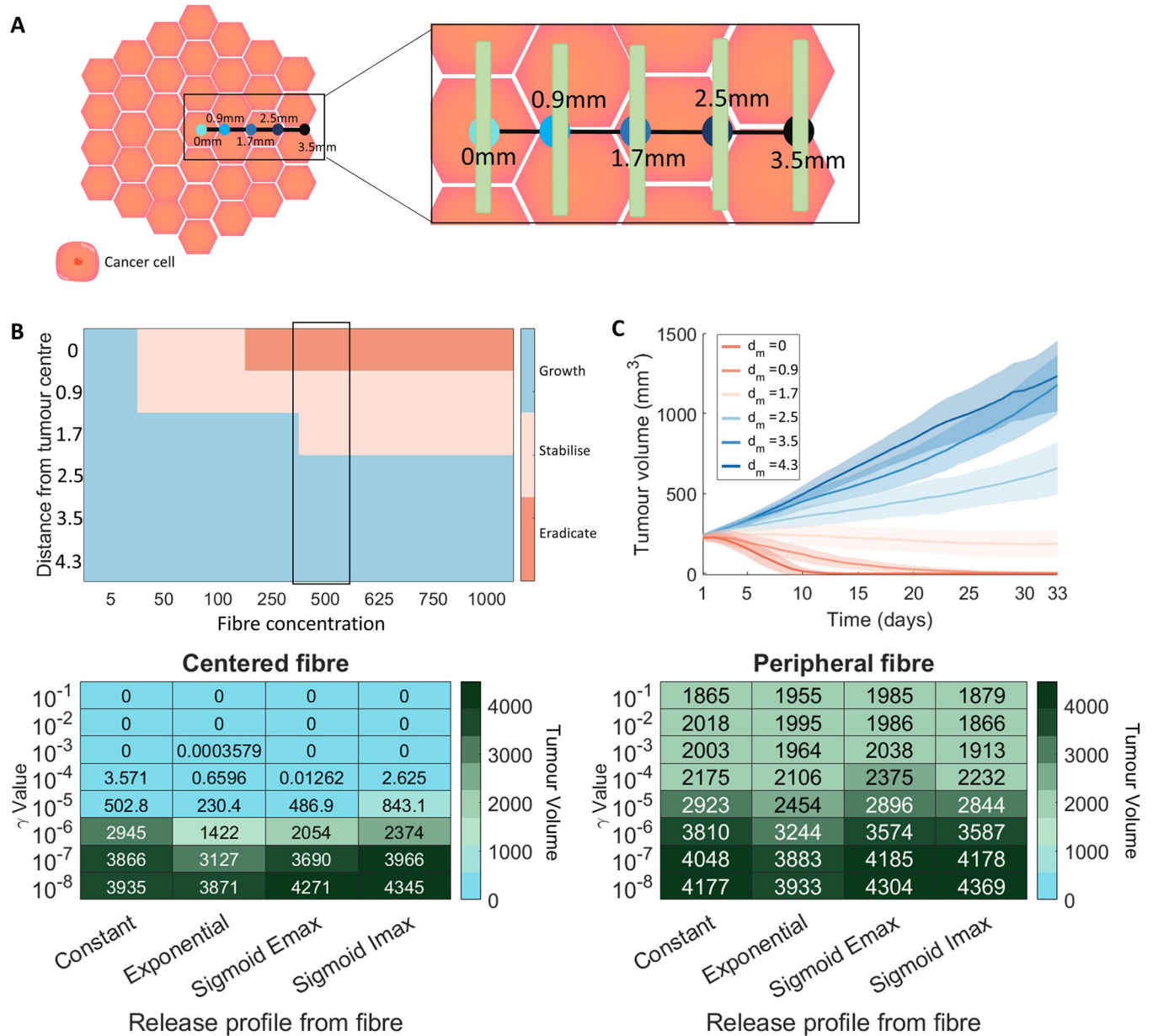


**Fig 6. Comparison of different fibre release and placement options.** (A) Tumour growth was investigated under different gemcitabine-loaded fibre placements  $d_m$ : central, 0.9 mm from centre, 1.7 mm from centre, 2.5 mm from centre, 3.5 mm from centre and 4.3 mm from centre. Locations of fibres on tumour surface for single implantations is depicted schematically. (B) A heatmap for the averaged final state of a tumour after 33 days of simulation for different initial injection concentrations and fibre placements. “Eradicate” denotes a tumour volume below  $1mm^3$ , “stabilise” denotes a tumour volume less than the initial tumour volume, and “growth” denotes a tumour volume greater than the initial tumour volume. (C) The mean (solid lines) and standard deviation (shades areas) of the tumour volume over 33 days for different fibre placement options with corresponding values highlighted in (B). (D) The tumour volume on day 33 for different release rates (indicated by the  $\gamma$  value) and release profiles with a central fibre placement. (E) The tumour volume on day 33 for different release rates (indicated by the  $\gamma$  value) and release profiles with a fibre placed on the edge of the tumour (3.5 mm away from centre). See **Section TS3 in S1 Technical Supplementary Information** for more details on these release functions. Legend for cell colouring: cancer cell (orange).

<https://doi.org/10.1371/journal.pcbi.1010104.g006>

driver of tumour growth in our model was the rate of cell mitosis. The idea that the cell cycling time is a fundamental part of tumour progression has been found in other mathematical models [103], suggesting that the model’s sensitivity in terms of tumour volume is in line with other models in the literature. It is also known that molecules can modulate the cell cycle of

cancer cells, changing the cancer aggressivity. For example, melatonin is a hormone known for its antitumour efficacy as it significantly increases the duration of the cell cycle of human breast cancer cells [104]. Given a heterogeneous cohort of individuals with varying degrees of tumour growth rates, our model suggests that the driver of these differences is most likely the cell cycling rate. Drugs targeting this should, therefore, be considered.

Depending on the cancer type, administering an intratumoural injection of a drug can be extremely difficult and administering treatments on the periphery can be an easier course of action. Simulating the model, we found that intratumoural administration of gemcitabine-loaded fibres significantly outperforms peritumoural administration. However, there is a threshold distance from the tumour to achieve an effective treatment, beyond which placing fibres further into the tumour bulk sees no added benefit. There is a clear benefit to increasing the dosage multiplicity and spreading the administered drug out amongst the tumour compared to a single high dose. Tumour volume was most significantly decreased when four free-drug point injections were administered compared to a single free-drug point injection. This proposes the existence of a potential threshold above which increasing the multiplicity of dosages or dosage size has a negligible effect over spreading out the dosages.

The location of the fibre and the total drug concentration in the fibre was a major driver of tumour eradication. For fibres located within the centre of the tumour with a significantly high drug concentration, it was possible to completely eradicate the tumour. Moving the fibre farther away from the centre, we found that there was no concentration of drug that would inhibit growth. This suggests that a large amount of drug from the implants is lost to the surrounding tissue, and this has detrimental effects on the efficacy of these devices. Fortunately, simulations show there is a minimal concentration of drug necessary for stabilisation, allowing these predictions to be used a way to guide dosage so that toxicity is minimised, and efficacy is maximised.

Interestingly, we found that changing the release profile of the drug from the device had a similar effect for fast enough release curves, i.e.  $\gamma$  between  $10^{-3}$  and  $\gamma^{-1}$ . This suggests that there is some margin of error for the creation of these devices and provides some promise for their optimisation.

More recently, research has been focused on combining gemcitabine with other drugs to improve its efficacy in the sustained-release devices. For example, nanoparticle albumin-bound paclitaxel (nab-paclitaxel) administered in combination with gemcitabine [9] is one of the standard of care treatment regimens that has shown an increase in overall survival in patients with advanced PDAC, as shown in a Phase I/II clinical trial [9]. A phase III clinical trial showed that gemcitabine and erlotinib also significantly increased overall survival in advanced PDAC patients compared to gemcitabine alone [105,106]. This drug combination has been investigated in an analogous sustained-release system by Wade *et al.* [13] and using this model, future work hopes to examine how the release profile of combination drugs such as this might be optimised.

Due to wanting to reduce the computational complexity of the VCBM, we made some simplifying assumptions that have introduced limitations into our model. To avoid simulating excessively large numbers of cells, we have chosen to scale the spatial unit appropriately so that we simulate on the order of  $\sim 10^6$  cells. An improvement for this model, could be to parallelise the agent update step to increase the speed of the simulation. In addition, we consider only a 2-dimensional cross section of the tumour, which is a simplification given tumour's grow in 3-dimensional environments. While this is a simplification, since the measurements obtained by Wade *et al.* [13] only measure tumour dimensions in a 2-dimensional cross-section, i.e. width and length, we feel it is appropriate to model growth in 2 dimensions. In addition, since the large effects felt in 3 dimensions will be based on surrounding organ tissue, we feel that

since we model neighbouring tissue as having a homogenous effect on tumour growth, there would be no significant impact of extending our model to 3 dimensions. Lastly, we model cell uptake by point sink terms; however, a cell would uptake drug across its surface area through drug molecule binding and internalisation. It would be possible to model this by extending the framework from a single point uptake to a uniform uptake across a cell's defined Voronoi cell region.

There are considerable avenues for future extensions of this work, and we feel the platform we have built is easily extendable by other computational oncologists. In particular, future modelling could extend the model to account for the dense fibrotic nature of PDAC [101,102] and investigate the impact the release and delivery of drug. In addition, the model could be used to simulate the efficacy of dual drug-loaded polymer and verify whether improvements on the current treatment protocol exist. There are many applications of degradable polymeric drug delivery systems in cancer therapy [10], for example, Rezk *et al.* [10] developed a pH-sensitive polymeric carrier to study the local delivery of anticancer drug bortezomib. They fitted the release profile of the drug from their carrier system to a mathematical formalism. Using our pancreatic cancer growth VCBM, it would be possible to feed in their drug release mechanism and simulate the efficacy under alternative protocols and predict the remaining tumour volume. Lastly, while we did not consider gemcitabine resistance in our model, it does occur in PDAC [3,4]. A simple extension of the model could consider the impact of resistance on the performance of therapy like other works on resistance of chemotherapeutics using mathematical models [107,108].

## Conclusion

Treatment for cancers with a poor prognosis, such as PDAC, are in vital need of novel therapeutic approaches that provide sustained, heightened, localised drug concentrations. The computational platform developed in this work can recapitulate spatially heterogeneous tumour growth and treatment with the chemotherapy drug gemcitabine. Investigating the efficacy of gemcitabine released from a degradable polymeric fibre implant, we can suggest that a minimum dosage for maximum efficacy exists based on the location of the device within the tumour. Furthermore, certain release profiles are more effective than others, suggesting that the way in which drug is released from these devices is crucial to improving patient treatment. Moving forward, a study of this form could be used to help inform experimental design and be integrated into future device development.

## Supporting information

**S1 Text. Supplementary Tables and Figures.** Supplementary Tables and Figures that support results in the main text. Includes Tables A-E and Figs A-O.  
(DOCX)

**S1 Technical Supplementary Information. Supplementary Technical Information about the FVM discretization for the model as well as time-stepping details.** Includes Figs A-F.  
(DOCX)

**S1 Code Documentation. Details of the functions within the C++ code for the model.** Corresponds to the code on Github.  
(DOCX)

## Author Contributions

**Conceptualization:** Adrienne L. Jenner, Peter S. Kim, Samantha J. Wade, Kara L. Vine.

**Data curation:** Samantha J. Wade, Kara L. Vine.

**Formal analysis:** Adrienne L. Jenner, Isobelle Parfitt, Dominic Steinitz, Pantea Pooladvand.

**Investigation:** Adrienne L. Jenner, Isobelle Parfitt.

**Methodology:** Adrienne L. Jenner, Wayne Kelly, Michael Dallaston, Dominic Steinitz.

**Software:** Wayne Kelly.

**Supervision:** Robyn Araujo, Peter S. Kim.

**Validation:** Pantea Pooladvand.

**Writing – original draft:** Adrienne L. Jenner, Michael Dallaston, Peter S. Kim.

**Writing – review & editing:** Adrienne L. Jenner, Robyn Araujo, Peter S. Kim, Samantha J. Wade, Kara L. Vine.

## References

1. Heinemann V (2001) Gemcitabine: progress in the treatment of pancreatic cancer. *Oncology* 60:8–18 <https://doi.org/10.1159/000055290> PMID: 11150902
2. Burris 3rd HA, Moore MJ, Andersen J, Green MR, Rothenberg ML, Modiano MR, et al (1997) Improvements in survival and clinical benefit with gemcitabine as first-line therapy for patients with advanced pancreas cancer: a randomized trial. *J Clin Oncol* 15:2403–2413 <https://doi.org/10.1200/JCO.1997.15.6.2403> PMID: 9196156
3. Andersson R, Aho U, Nilsson BI, Peters GJ, Pastor–Anglada M, Rasch W, et al (2009) Gemcitabine chemoresistance in pancreatic cancer: molecular mechanisms and potential solutions. *Scand J Gastroenterol* 44:782–786 <https://doi.org/10.1080/00365520902745039> PMID: 19214867
4. Akada M, Crnogorac–Jurcevic T, Lattimore S, Mahon P, Lopes R, Sunamura M, et al (2005) Intrinsic chemoresistance to gemcitabine is associated with decreased expression of BNIP3 in pancreatic cancer. *Clin Cancer Res* 11:3094–3101 <https://doi.org/10.1158/1078-0432.CCR-04-1785> PMID: 15837765
5. de Sousa Cavalcante L, Monteiro G (2014) Gemcitabine: metabolism and molecular mechanisms of action, sensitivity and chemoresistance in pancreatic cancer. *Eur J Pharmacol* 741:8–16 <https://doi.org/10.1016/j.ejphar.2014.07.041> PMID: 25084222
6. Cappella P, Tomasoni D, Faretta M, Lupi M, Montalenti F, Viale F, et al (2001) Cell cycle effects of gemcitabine. *Int J cancer* 93:401–408 <https://doi.org/10.1002/ijc.1351> PMID: 11433406
7. Abrams MJ, Rakszawski K, Vasekar M, Passero F, Abbas A, Jia Y, et al (2016) Recent advances in pancreatic cancer: Updates and insights from the 2015 annual meeting of the American Society of Clinical Oncology. *Therap Adv Gastroenterol* 9:141–151 <https://doi.org/10.1177/1756283X15622601> PMID: 26929776
8. Toschi L, Finocchiaro G, Bartolini S, Gioia V, Cappuzzo F (2005) Role of gemcitabine in cancer therapy.
9. Von Hoff DD, Ervin T, Arena FP, Chiorean EG, Infante J, Moore M, et al (2013) Increased survival in pancreatic cancer with nab–paclitaxel plus gemcitabine. *N Engl J Med* 369:1691–1703 <https://doi.org/10.1056/NEJMoa1304369> PMID: 24131140
10. Rezk AI, Obiweluozor FO, Choukrani G, Park CH, Kim CS (2019) Drug release and kinetic models of anticancer drug (BTZ) from a pH–responsive alginate polydopamine hydrogel: Towards cancer chemotherapy. *Int J Biol Macromol* 141:388–400 <https://doi.org/10.1016/j.ijbiomac.2019.09.013> PMID: 31493453
11. Nazir S, Khan MUA, Al–Arjan WS, Abd Razak SI, Javed A, Kadir MRA (2021) Nanocomposite hydrogels for melanoma skin cancer care and treatment: In–vitro drug delivery, drug release kinetics and anti–cancer activities. *Arab J Chem* 14:103120
12. Kearney CJ, Mooney DJ (2013) Macroscale delivery systems for molecular and cellular payloads. *Nat Mater* 12:1004–1017 <https://doi.org/10.1038/nmat3758> PMID: 24150418
13. Wade SJ, Sahin Z, Piper A–K, Talebian S, Aghmesheh M, Foroughi J, et al (2020) Dual Delivery of Gemcitabine and Paclitaxel by Wet–Spun Coaxial Fibers Induces Pancreatic Ductal Adenocarcinoma Cell Death, Reduces Tumor Volume, and Sensitizes Cells to Radiation. *Adv Healthc Mater* 9:2001115 <https://doi.org/10.1002/adhm.202001115> PMID: 33000905

14. Wade SJ, Zuzic A, Foroughi J, Talebian S, Aghmesheh M, Moulton SE, et al (2017) Preparation and in vitro assessment of wet-spun gemcitabine-loaded polymeric fibers: Towards localized drug delivery for the treatment of pancreatic cancer. *Pancreatology* 17:795–804
15. Lee KY, Mooney DJ (2012) Alginate: Properties and biomedical applications. *Prog Polym Sci* 37:106–126 <https://doi.org/10.1016/j.progpolymsci.2011.06.003> PMID: 22125349
16. Wade SJ (2019) Fabrication and preclinical assessment of drug eluting wet spun fibres for pancreatic cancer treatment.
17. Louzoun Y, Xue C, Lesinski GB, Friedman A (2014) A mathematical model for pancreatic cancer growth and treatments. *J Theor Biol* 351:74–82 <https://doi.org/10.1016/j.jtbi.2014.02.028> PMID: 24594371
18. Liu J, Wang XS (2019) Numerical optimal control of a size-structured PDE model for metastatic cancer treatment. *Math Biosci* 314:28–42 <https://doi.org/10.1016/j.mbs.2019.06.001> PMID: 31176704
19. Lai X, Friedman A (2019) Mathematical modeling in scheduling cancer treatment with combination of VEGF inhibitor and chemotherapy drugs. *J Theor Biol* 462:490–498 <https://doi.org/10.1016/j.jtbi.2018.11.018> PMID: 30468760
20. Ghasemi M, Sivaloganathan S (2020) A computational study of combination HIFU-chemotherapy as a potential means of overcoming cancer drug resistance. *Math Biosci* 329:108456 <https://doi.org/10.1016/j.mbs.2020.108456> PMID: 32841615
21. Rockne RC, Hawkins-Daarud A, Swanson KR, Sluka JP, Glazier JA, Macklin P, et al (2019) The 2019 mathematical oncology roadmap. *Phys Biol* 16:41005 <https://doi.org/10.1088/1478-3975/ab1a09> PMID: 30991381
22. Dogra P, Butner JD, Chuang Y, Caserta S, Goel S, Brinker CJ, et al (2019) Mathematical modeling in cancer nanomedicine: a review. *Biomed Microdevices* 21:1–23 <https://doi.org/10.1007/s10544-019-0380-2> PMID: 30949850
23. Gallaher JA, Enriquez-Navas PM, Luddy KA, Gatenby RA, Anderson ARA (2017) Spatial heterogeneity and evolutionary dynamics modulate time to recurrence in continuous and adaptive cancer therapies. *bioRxiv* 78:2127–2139
24. Gallaher JA, Massey SC, Hawkins-Daarud A, Noticewala SS, Rockne RC, Johnston SK, et al (2020) From cells to tissue: How cell scale heterogeneity impacts glioblastoma growth and treatment response. *PLoS Comput Biol* 16:e1007672 <https://doi.org/10.1371/journal.pcbi.1007672> PMID: 32101537
25. Macnamara CK (2021) Biomechanical modelling of cancer: Agent-based force-based models of solid tumours within the context of the tumour microenvironment. *Comput Syst Oncol* 1:e1018
26. Macnamara CK, Caiazzo A, Ramis-Conde I, Chaplain MAJ (2020) Computational modelling and simulation of cancer growth and migration within a 3D heterogeneous tissue: The effects of fibre and vascular structure. *J Comput Sci* 40:101067
27. Szymańska Z, Cytowski M, Mitchell E, Macnamara CK, Chaplain MAJ (2018) Computational Modelling of Cancer Development and Growth: Modelling at Multiple Scales and Multiscale Modelling. *Bull Math Biol* 80:1366–1403 <https://doi.org/10.1007/s11538-017-0292-3> PMID: 28634857
28. de Montigny J, Iosif A, Breitwieser L, Manca M, Bauer R, Vavourakis V (2021) An in silico hybrid continuum-agent-based procedure to modelling cancer development: Interrogating the interplay amongst glioma invasion, vascularity and necrosis. *Methods* 185:94–104 <https://doi.org/10.1016/j.ymeth.2020.01.006> PMID: 31981608
29. Cess CG, Finley SD (2020) Multi-scale modeling of macrophage-T cell interactions within the tumor microenvironment. *PLoS Comput Biol* 16:e1008519 <https://doi.org/10.1371/journal.pcbi.1008519> PMID: 33362239
30. Cess CG, Finley SD (2022) Multiscale modeling of tumor adaption and invasion following anti-angiogenic therapy. *Comput Syst Oncol* 2:e1032
31. Phillips CM, Lima EABF, Woodall RT, Brock A, Yankeelov TE (2020) A hybrid model of tumor growth and angiogenesis: In silico experiments. *PLoS One* 15:e0231137 <https://doi.org/10.1371/journal.pone.0231137> PMID: 32275674
32. Klows JJ, Browning AP, Murphy RJ, Carr EJ, Plank MJ, Gunasingh G, et al (2022) A stochastic mathematical model of 4D tumour spheroids with real-time fluorescent cell cycle labelling. *J R Soc Interface* 19:20210903 <https://doi.org/10.1098/rsif.2021.0903> PMID: 35382573
33. Wodarz D, Hofacre A, Lau JW, Sun Z, Fan H, Komarova NL (2012) Complex spatial dynamics of oncolytic viruses in vitro: mathematical and experimental approaches. *PLoS Comput Biol* 8:e1002547 <https://doi.org/10.1371/journal.pcbi.1002547> PMID: 22719239

34. Gong C, Milberg O, Wang B, Vicini P, Narwal R, Roskos L, et al (2017) A computational multiscale agent-based model for simulating spatio-temporal tumour immune response to PD1 and PDL1 inhibition. *J R Soc Interface* 14:20170320 <https://doi.org/10.1098/rsif.2017.0320> PMID: 28931635
35. Benmir M, Chabbar S, Aboulaich R, Ismaili N, Benmir M, Chabbar S, et al (2022) A Hybrid Model of Tumor Growth Under Chemotherapy Medicine To cite this version: HAL Id: hal-03715363 A Hybrid Model of Tumor Growth Under Chemotherapy Medicine.
36. Cockrell C, Axelrod DE (2019) Optimization of Dose Schedules for Chemotherapy of Early Colon Cancer Determined by High-Performance Computer Simulations. *Cancer Inform.* <https://doi.org/10.1177/1176935118822804> PMID: 30675100
37. Stace REA, Stiehl T, Chaplain MAJ, Marciniak-Czochra A, Lorenzi T (2020) Discrete and continuum phenotype-structured models for the evolution of cancer cell populations under chemotherapy. *Math Model Nat Phenom.* <https://doi.org/10.1051/mmnp/2019027>
38. Tang L, Van De Ven AL, Guo D, Andasari V, Cristini V, Li KC, et al (2014) Computational modeling of 3D tumor growth and angiogenesis for chemotherapy evaluation. *PLoS One* 9:1–12 <https://doi.org/10.1371/journal.pone.0083962> PMID: 24404145
39. Wang Z, Butner JD, Cristini V, Deisboeck TS (2015) Integrated PK-PD and agent-based modeling in oncology. *J Pharmacokinetic Pharmacodyn* 42:179–189 <https://doi.org/10.1007/s10928-015-9403-7> PMID: 25588379
40. Pourhasanzade F, Sabzpoushan SH (2019) A cellular automata model of chemotherapy effects on tumour growth: targeting cancer and immune cells. *Math Comput Model Dyn Syst* 25:63–89
41. Arabameri A, Pourgholaminejad A (2021) Modeling codelivery of CD73 inhibitor and dendritic cell-based vaccines in cancer immunotherapy. *Comput Biol Chem* 95:107585 <https://doi.org/10.1016/j.compbiolchem.2021.107585> PMID: 34610532
42. Ozik J, Collier N, Wozniak JM, Macal C, Cockrell C, Friedman SH, et al (2018) High-throughput cancer hypothesis testing with an integrated PhysiCell-EMEWS workflow. *BMC Bioinformatics.* <https://doi.org/10.1186/s12859-018-2510-x> PMID: 30577742
43. Ghaffarizadeh A, Heiland R, Friedman SH, Mumenthaler SM, Macklin P (2018) PhysiCell: An open source physics-based cell simulator for 3-D multicellular systems. *PLoS Comput Biol* 14:e1005991 <https://doi.org/10.1371/journal.pcbi.1005991> PMID: 29474446
44. Rocha HL, Godet I, Kurtoglu F, Metzcar J, Konstantinopoulos K, Bhojar S, et al (2021) A persistent invasive phenotype in post-hypoxic tumor cells is revealed by fate mapping and computational modeling. *iScience* 24:102935 <https://doi.org/10.1016/j.isci.2021.102935> PMID: 34568781
45. Jenner A, Smalley M, Goldman D, Lawler S, Goldman A, Macklin P, et al (2021) Stromal density shapes the response to HSV-1 oncolytic virus rQNestin in brain tumours. Submitted
46. Chen J, Vermolen FJ (2021) Several Agent-Based and Cellular Automata Mathematical Frameworks for Modeling Pancreatic Cancer. In: *Numer. Math. Adv. Appl. ENUMATH 2019.* Springer, pp 265–274
47. Dogra P, Ramáirez JR, Peláez MJ, Wang Z, Cristini V, Parasher G, et al (2020) Mathematical modeling to address challenges in pancreatic cancer. *Curr Top Med Chem* 20:367–376 <https://doi.org/10.2174/1568026620666200101095641> PMID: 31893993
48. Arifin DY, Lee LY, Wang CH (2006) Mathematical modeling and simulation of drug release from microspheres: Implications to drug delivery systems. *Adv Drug Deliv Rev* 58:1274–1325 <https://doi.org/10.1016/j.addr.2006.09.007> PMID: 17097189
49. Lao LL, Peppas NA, Boey FYC, Venkatraman SS (2011) Modeling of drug release from bulk-degrading polymers. *Int J Pharm* 418:28–41 <https://doi.org/10.1016/j.ijpharm.2010.12.020> PMID: 21182912
50. Siepmann J, Siepmann F (2012) Modeling of diffusion controlled drug delivery. *J Control Release* 161:351–362 <https://doi.org/10.1016/j.jconrel.2011.10.006> PMID: 22019555
51. Casalini T, Rossi F, Lazzari S, Perale G, Masi M (2014) Mathematical modeling of PLGA microparticles: From polymer degradation to drug release. *Mol Pharm* 11:4036–4048 <https://doi.org/10.1021/mp500078u> PMID: 25230105
52. McGinty S, King D, Pontrelli G (2017) Mathematical modelling of variable porosity coatings for controlled drug release. *arXiv* 45:51–60 <https://doi.org/10.1016/j.medengphy.2017.04.006> PMID: 28461200
53. Jenner AL, Frascoli F, Yun CO, Kim PS (2020) Optimising hydrogel release profiles for viro-immunotherapy using oncolytic adenovirus expressing IL-12 and GM-CSF with immature dendritic cells. *Appl Sci* 10:2872
54. Kalkhoran AHZ, Vahidi O, Naghib SM (2018) A new mathematical approach to predict the actual drug release from hydrogels. *Eur J Pharm Sci* 111:303–310 <https://doi.org/10.1016/j.ejps.2017.09.038> PMID: 28962856

55. Manga RD, Jha PK (2017) Mathematical models for controlled drug release through pH-responsive polymeric hydrogels. *J Pharm Sci* 106:629–638 <https://doi.org/10.1016/j.xphs.2016.10.019> PMID: 27890245
56. Spiridonova TI, Tverdokhlebov SI, Anissimov YG (2019) Investigation of the Size Distribution for Diffusion-Controlled Drug Release From Drug Delivery Systems of Various Geometries. *J Pharm Sci* 108:2690–2697 <https://doi.org/10.1016/j.xphs.2019.03.036> PMID: 30980858
57. Jenner AL, Frascoli F, Coster ACF, Kim PS (2020) Enhancing oncolytic virotherapy: Observations from a Voronoi Cell-Based model. *J Theor Biol.* <https://doi.org/10.1016/j.jtbi.2019.110052> PMID: 31626813
58. Ghaffarizadeh A, Friedman SH, MacKlin P (2016) BioFVM: An efficient, parallelized diffusive transport solver for 3-D biological simulations. *Bioinformatics* 32:1256–1258 <https://doi.org/10.1093/bioinformatics/btv730> PMID: 26656933
59. Petlin DG, Rybachuk M, Anissimov YG (2015) Pathway Distribution Model for Solute Transport in Stratum Corneum. *J Pharm Sci* 104:4443–4447 <https://doi.org/10.1002/jps.24669> PMID: 26506429
60. Petlin DG, Amarah AA, Tverdokhlebov SI, Anissimov YG (2017) A fiber distribution model for predicting drug release rates. *J Control Release* 258:218–225 <https://doi.org/10.1016/j.jconrel.2017.05.021> PMID: 28526437
61. Kaunisto E, Marucci M, Borgquist P, Axelsson A (2011) Mechanistic modelling of drug release from polymer-coated and swelling and dissolving polymer matrix systems. *Int J Pharm* 418:54–77 <https://doi.org/10.1016/j.ijpharm.2011.01.021> PMID: 21256939
62. Pasdunkorale A J, Turner IW (2005) A second order control-volume finite-element least-squares strategy for simulating diffusion in strongly anisotropic media. *J Comput Math* 1–16
63. Chaudhry QA, Abbas A, Noor A, Asif M (2019) In silico modeling for the risk assessment of toxicity in cells. *Comput & Math with Appl* 77:1541–1548
64. Shakeri F, Dehghan M (2011) The finite volume spectral element method to solve Turing models in the biological pattern formation. *Comput & Math with Appl* 62:4322–4336
65. Andasari V, Gerisch A, Lolas G, South AP, Chaplain MAJ (2011) Mathematical modeling of cancer cell invasion of tissue: biological insight from mathematical analysis and computational simulation. *J Math Biol* 63:141–171 <https://doi.org/10.1007/s00285-010-0369-1> PMID: 20872264
66. Hubbard ME, Byrne HM (2013) Multiphase modelling of vascular tumour growth in two spatial dimensions. *J Theor Biol* 316:70–89 <https://doi.org/10.1016/j.jtbi.2012.09.031> PMID: 23032218
67. Eymard R, Gallouët T, Herbin R (2000) Finite volume methods. *Handb Numer Anal* 7:713–1018
68. Khalid S, Chaudhry QA (2019) Quantitative analysis of cancer risk assessment in a mammalian cell with the inclusion of mitochondria. *Comput & Math with Appl* 78:2449–2467
69. Ain K, Wibowo RA, Soelistono S (2017) Modeling of electrical impedance tomography to detect breast cancer by finite volume methods. In: *J. Phys. Conf. Ser.* p 12001
70. Storey KM, Jackson TL (2021) An Agent-Based Model of Combination Oncolytic Viral Therapy and Anti-PD-1 Immunotherapy Reveals the Importance of Spatial Location When Treating Glioblastoma. *Cancers (Basel)* 13:5314 <https://doi.org/10.3390/cancers13215314> PMID: 34771476
71. Haroske G, Dimmer V, Steindorf D, Schilling U, Theissig F, Kunze KD (1996) Cellular sociology of proliferating tumor cells in invasive ductal breast cancer. *Anal Quant Cytol Histol* 18:191–198 PMID: 8790831
72. Bock M, Tyagi AK, Kreft J-U, Alt W (2010) Generalized voronoi tessellation as a model of two-dimensional cell tissue dynamics. *Bull Math Biol* 72:1696–1731 <https://doi.org/10.1007/s11538-009-9498-3> PMID: 20082148
73. Saribudak A, Kucharavy H, Hubbard K, Uyar MÜ (2016) Spatial Heterogeneity Analysis in Evaluation of Cell Viability and Apoptosis for Colorectal Cancer Cells. *IEEE J Transl Eng Heal Med* 4:1–9 <https://doi.org/10.1109/JTEHM.2016.2578331> PMID: 27574578
74. Lin L, Wang X, Zeng X (2014) Geometrical modeling of cell division and cell remodeling based on Voronoi tessellation method. *C Comput Model Eng & Sci* 98:203–220
75. Saribudak A, Dong Y, Gundry S, Hsieh J, Uyar MÜ (2015) Mathematical models of tumor growth using Voronoi tessellations in pathology slides of kidney cancer. In: 2015 37th Annu. Int. Conf. IEEE Eng. Med. Biol. Soc. pp 4454–4457 <https://doi.org/10.1109/EMBC.2015.7319383> PMID: 26737283
76. Maier HJ, Wirth T, Beug H (2010) Epithelial-mesenchymal transition in pancreatic carcinoma. *Cancers (Basel)* 2:2058–2083
77. Luu T (2021) Epithelial-mesenchymal transition and its regulation mechanisms in pancreatic cancer. *Front Oncol* 11:1228 <https://doi.org/10.3389/fonc.2021.646399> PMID: 33928036



78. Karamitopoulou E (2013) Role of epithelial–mesenchymal transition in pancreatic ductal adenocarcinoma: is tumor budding the missing link? *Front Oncol* 3:221 <https://doi.org/10.3389/fonc.2013.00221> PMID: 24062980
79. Bulle A, Lim K–H (2020) Beyond just a tight fortress: contribution of stroma to epithelial–mesenchymal transition in pancreatic cancer. *Signal Transduct Target Ther* 5:1–12
80. Buijs JO den, Musters M, Verrips T, Post JA, Braam B, Van Riel N (2004) Mathematical modeling of vascular endothelial layer maintenance: the role of endothelial cell division, progenitor cell homing, and telomere shortening. *Am J Physiol Circ Physiol* 287:H2651–H2658 <https://doi.org/10.1152/ajpheart.00332.2004> PMID: 15284068
81. Lobo EP (2014) Modelling the Role of Interclonal Cooperativity During Early Carcinogenesis. University of Sydney
82. Kansal AR, Torquato S, Harsh GR, Chiocca EA, Deisboeck TS (2000) Simulated brain tumor growth dynamics using a three–dimensional cellular automaton. *J Theor Biol* 203:367–382 <https://doi.org/10.1006/jtbi.2000.2000> PMID: 10736214
83. Jiao Y, Torquato S (2011) Emergent behaviors from a cellular automaton model for invasive tumor growth in heterogeneous microenvironments. *PLoS Comput Biol* 7:e1002314 <https://doi.org/10.1371/journal.pcbi.1002314> PMID: 22215996
84. Streichan SJ, Hoerner CR, Schneidt T, Holzer D, Hufnagel L (2014) Spatial constraints control cell proliferation in tissues. *Proc Natl Acad Sci* 111:5586–5591 <https://doi.org/10.1073/pnas.1323016111> PMID: 24706777
85. Delarue M, Montel F, Vignjevic D, Prost J, Joanny J–F, Cappello G (2014) Compressive stress inhibits proliferation in tumor spheroids through a volume limitation. *Biophys J* 107:1821–1828 <https://doi.org/10.1016/j.bpj.2014.08.031> PMID: 25418163
86. Levayer R (2020) Solid stress, competition for space and cancer: The opposing roles of mechanical cell competition in tumour initiation and growth. In: *Semin. Cancer Biol.* pp 69–80 <https://doi.org/10.1016/j.semcancer.2019.05.004> PMID: 31077845
87. Crosley P, Farkkila A, Jenner AL, Burlot C, Cardinal O, Potts KG, et al (2021) Procaspace–Activating Compound–1 Synergizes with TRAIL to Induce Apoptosis in Established Granulosa Cell Tumor Cell Line (KGN) and Explanted Patient Granulosa Cell Tumor Cells In Vitro. *Int J Mol Sci* 22:4699 <https://doi.org/10.3390/ijms22094699> PMID: 33946730
88. Kalvass JC, Pollack GM (2007) Kinetic considerations for the quantitative assessment of efflux activity and inhibition: implications for understanding and predicting the effects of efflux inhibition. *Pharm Res* 24:265–276 <https://doi.org/10.1007/s11095-006-9135-x> PMID: 17191095
89. Pena–Miller R, Laehnemann D, Jansen G, Fuentes–Hernandez A, Rosenstiel P, Schulenburg H, et al (2013) When the Most Potent Bacterial Combination Selects for the Greatest Bacterial Load: The Smile–Frown Transition. *PLoS Biol* 11:14–16 <https://doi.org/10.1371/journal.pbio.1001540> PMID: 23630452
90. Minto CF, Schnider TW, Short TG, Gregg KM, Gentilini A, Shafer SL (2000) Response surface model for anesthetic drug interactions. *Anesthesiology* 92:1603–1616 <https://doi.org/10.1097/0000542-200006000-00017> PMID: 10839909
91. Li Z, Tian T, Lv F, Chang Y, Wang X, Zhang L, et al (2013) Six1 Promotes Proliferation of Pancreatic Cancer Cells via Upregulation of Cyclin D1 Expression. *PLoS One*. <https://doi.org/10.1371/journal.pone.0059203> PMID: 23527134
92. Sinha A, Cherba D, Bartlam H, Lenkiewicz E, Evers L, Barrett MT, et al (2014) Mesenchymal–like pancreatic cancer cells harbor specific genomic alterations more frequently than their epithelial–like counterparts. *Mol Oncol* 8:1253–1265 <https://doi.org/10.1016/j.molonc.2014.04.007> PMID: 24837184
93. Zhou P, Li B, Liu F, Zhang M, Wang Q, Liu Y, et al (2017) The epithelial to mesenchymal transition (EMT) and cancer stem cells: implication for treatment resistance in pancreatic cancer. *Mol Cancer* 16:1–11
94. Chan T–S, Shaked Y, Tsai KK (2019) Targeting the interplay between cancer fibroblasts, mesenchymal stem cells, and cancer stem cells in desmoplastic cancers. *Front Oncol* 9:688 <https://doi.org/10.3389/fonc.2019.00688> PMID: 31417869
95. Wells DK, Chuang Y, Knapp LM, Brockmann D, Kath WL, Leonard JN (2015) Spatial and Functional Heterogeneities Shape Collective Behavior of Tumor–Immune Networks. *PLoS Comput Biol*. <https://doi.org/10.1371/journal.pcbi.1004181> PMID: 25905470
96. Wang S, Huang S, Sun YL (2017) Epithelial–mesenchymal transition in pancreatic cancer: a review. *Biomed Res. Int.* 2017: <https://doi.org/10.1155/2017/2646148> PMID: 29379795

97. Upton RN, Mould DR (2014) Basic concepts in population modeling, simulation, and model-based drug development: Part 3—introduction to pharmacodynamic modeling methods. *CPT Pharmacometrics Syst Pharmacol* 3:1–16 <https://doi.org/10.1038/psp.2013.71> PMID: 24384783
98. Gabrielsson J, Andersson R, Jirstrand M, Hjorth S (2019) Dose–response–time data analysis: an underexploited trinity. *Pharmacol Rev* 71:89–122 <https://doi.org/10.1124/pr.118.015750> PMID: 30587536
99. Prinz H (2010) Hill coefficients, dose—response curves and allosteric mechanisms. *J Chem Biol* 3:37–44 <https://doi.org/10.1007/s12154-009-0029-3> PMID: 19779939
100. Hardacre JM, Mulcahy M, Small W, Talamonti M, Obel J, Krishnamurthi S, et al (2013) Addition of algenpantucel–L immunotherapy to standard adjuvant therapy for pancreatic cancer: a phase 2 study. *J Gastrointest Surg* 17:94–101 <https://doi.org/10.1007/s11605-012-2064-6> PMID: 23229886
101. Perez VM, Kearney JF, Yeh JJ (2021) The PDAC Extracellular Matrix: A Review of the ECM Protein Composition, Tumor Cell Interaction, and Therapeutic Strategies. *Front Oncol* 11:114114 <https://doi.org/10.3389/fonc.2021.751311> PMID: 34692532
102. Xie D, Xie K (2015) Pancreatic cancer stromal biology and therapy. *Genes & Dis* 2:133–143 <https://doi.org/10.1016/j.gendis.2015.01.002> PMID: 26114155
103. Crivelli JJ, Földes J, Kim PS, Wares JR (2012) A mathematical model for cell cycle–specific cancer vir- otherapy. *J Biol Dyn* 6:104–120 <https://doi.org/10.1080/17513758.2011.613486> PMID: 22873678
104. Cos S, Recio J, Sánchez–Barceló EJ (1996) Modulation of the length of the cell cycle time of MCF–7 human breast cancer cells by melatonin. *Life Sci* 58:811–816 [https://doi.org/10.1016/0024-3205\(95\)02359-3](https://doi.org/10.1016/0024-3205(95)02359-3) PMID: 8632728
105. Conroy T, Hammel P, Hebbar M, Ben Abdelghani M, Wei AC, Raoul J– L, et al (2018) FOLFIRINOX or gemcitabine as adjuvant therapy for pancreatic cancer. *N Engl J Med* 379:2395–2406 <https://doi.org/10.1056/NEJMoa1809775> PMID: 30575490
106. Moore MJ, Goldstein D, Hamm J, Figer A, Hecht JR, Gallinger S, et al (2007) Erlotinib plus gemcita- bine compared with gemcitabine alone in patients with advanced pancreatic cancer: a phase III trial of the National Cancer Institute of Canada Clinical Trials Group. *J Clin Oncol* 25:1960–1966 <https://doi.org/10.1200/JCO.2006.07.9525> PMID: 17452677
107. Craig M, Jenner AL, Namgung B, Lee LP, Goldman A (2020) Engineering in Medicine to Address the Challenge of Cancer Drug Resistance: From Micro: From Nanotechnologies to Computational and Mathematical Modeling. *Chem Rev*. <https://doi.org/10.1021/acs.chemrev.0c00356>
108. Cassidy T, Nichol D, Robertson–Tessi M, Craig M, Anderson ARA (2021) The role of memory in non– genetic inheritance and its impact on cancer treatment resistance. *PLoS Comput Biol* 17:e1009348 <https://doi.org/10.1371/journal.pcbi.1009348> PMID: 34460809